Electronic Supplementary Information (ESI) for Journal of Dalton Transactions

This journal is © The Royal Society of Chemistry 2017

SUPPORTING INFORMATION

Title: *Effect of Functional Groups in Aqueous-Phase Selective Sensing of Fe(III) Ions by Thienothiophene-Based Zirconium Metal-Organic Frameworks and its application in logic gate*

Author(s): Rana Dalapati, Ülkü Kökçam-Demir, Christoph Janiak, and Shyam Biswas*

Department of Chemistry, Indian Institute of Technology Guwahati, Guwahati, 781039 Assam, India

Institut für Anorganische Chemie und Strukturchemie, Universität Düsseldorf, Universitätsstraße 1, 40225 Düsseldorf, Germany

* To whom correspondence should be addressed. E-mail: sbiswas@iitg.ernet.in; Tel: 91-3612583309.

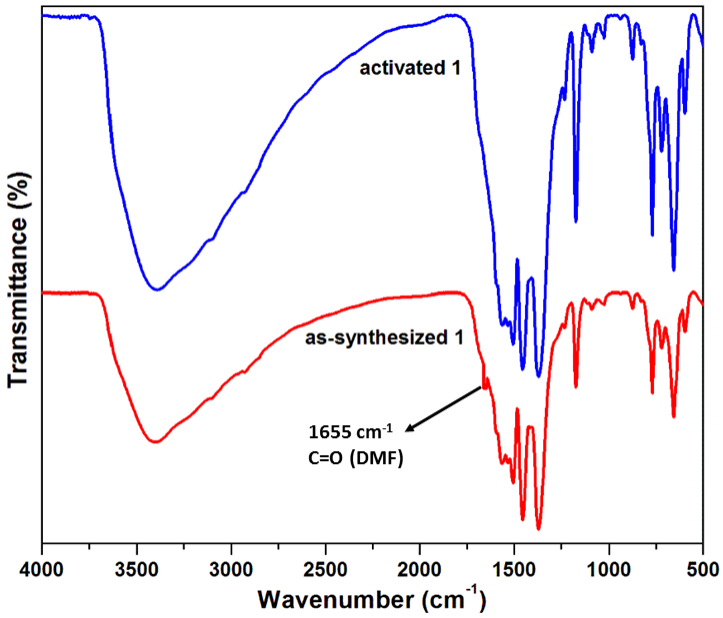

Figure S1. FT-IR spectra of as-synthesized and activated **1**.

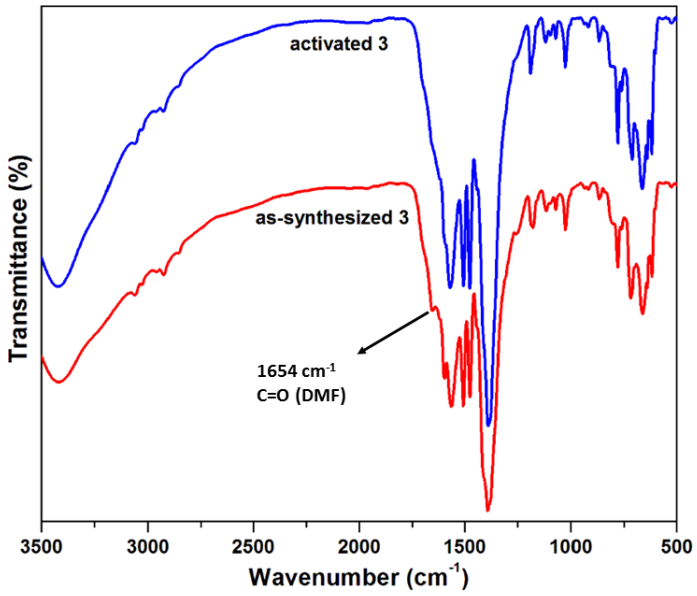

Figure S2. FT-IR spectra of as-synthesized and activated **3**.

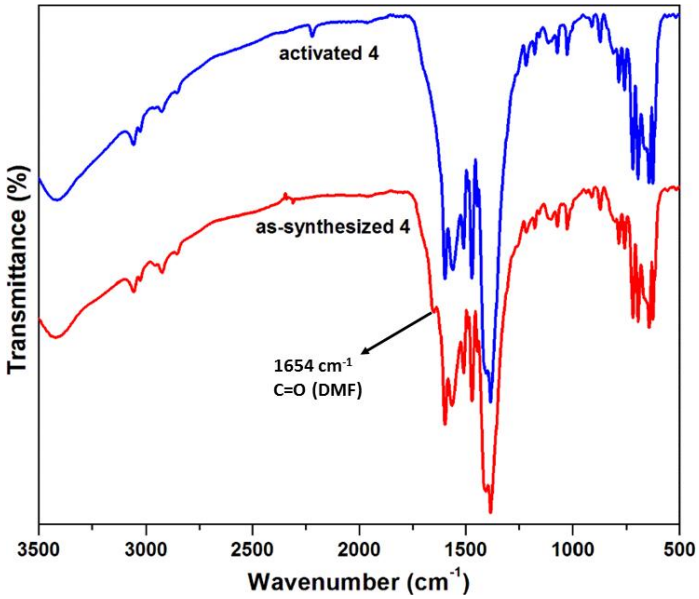

Figure S3. FT-IR spectra of as-synthesized and activated **4**.

Table S1. Lattice parameters of as-synthesized **1**, **3** and **4** having cubic unit cells. The values are compared with those of the formerly reported, isostructural, dimethyl-functionalized Zr(IV)-based compound.

Compound	*a* (Å)	*V* (Å^3)
1	23.0145(3)	12,190.0(7)
3	23.1153(3)	12,350.9(5)
4	22.9783(7)	12,132.6(12)
$[Zr_6O_4(OH)_4(DMTDC)_6]$[1]	23.0917(6)	12,313.1(3)
Zr-DMTDC[2]	23.12	12,358.43

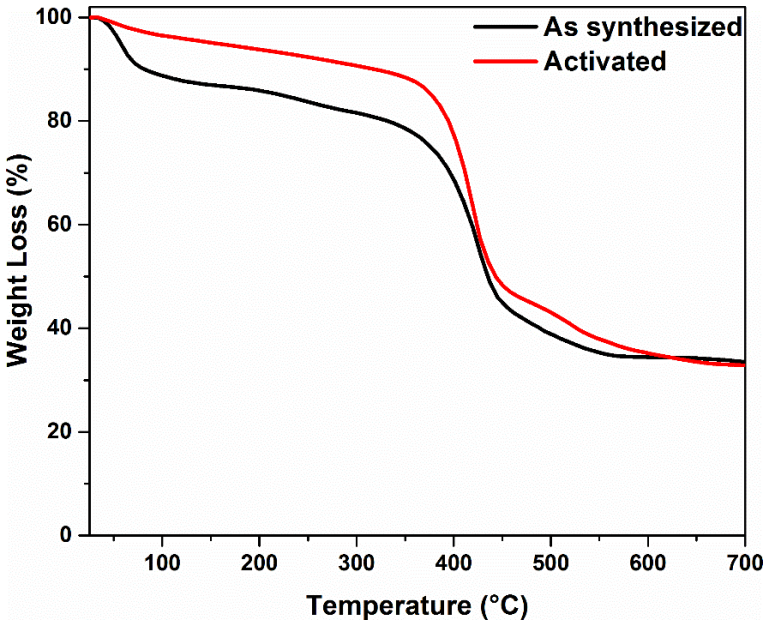

Figure S4. TG curves of **1** and **1'** recorded in an air atmosphere in the temperature range of 25-700 °C with a heating rate of 5 °C min^{-1}.

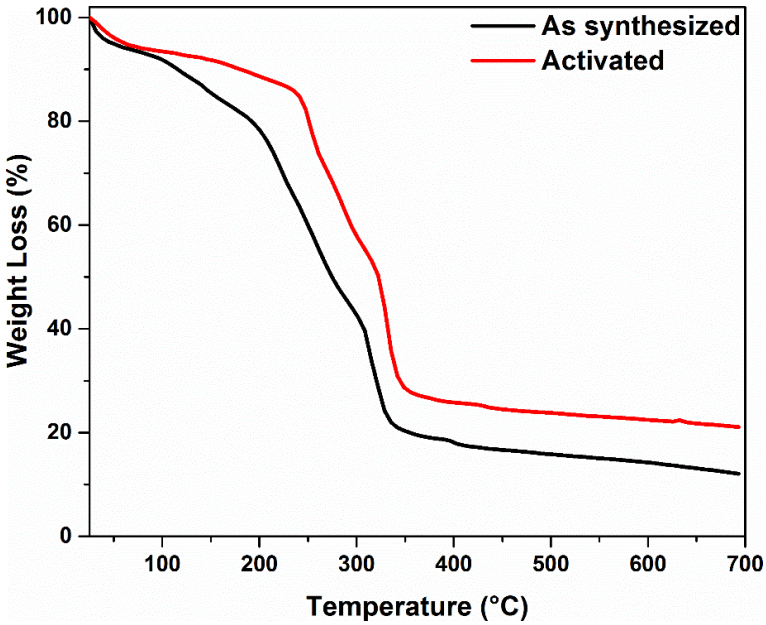

Figure S5. TG curves of **3** and **3'** recorded in an air atmosphere in the temperature range of 25-700 °C with a heating rate of 5 °C min^{-1}.

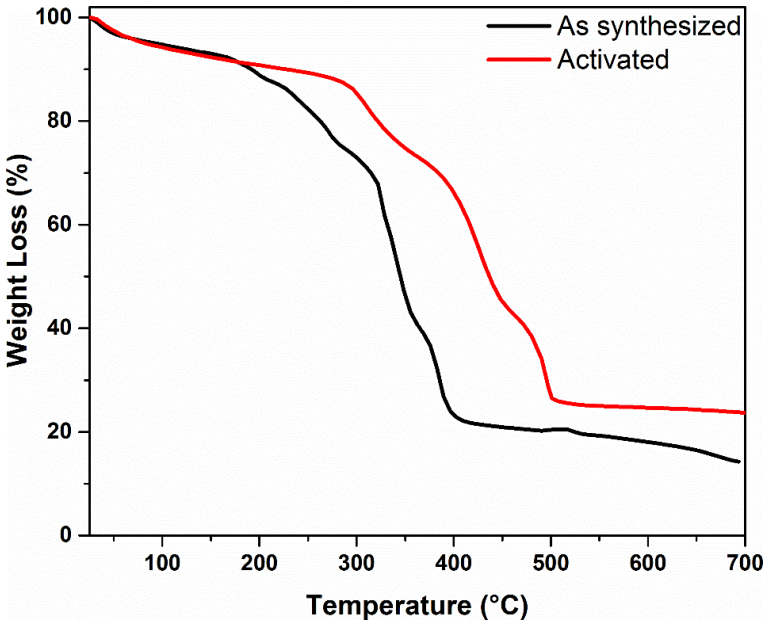

Figure S6. TG curves of **4** and **4'** recorded in an air atmosphere in the temperature range of 25-700 °C with a heating rate of 5 °C min^{-1}.

Table S2. Weight loss steps in the TG curves of as-synthesized **1**, **3** and **4**, and their assignments.

Compound	First Weight Loss (%): Obs. / Cal.	No. of H_2O Molecules Removed in First Weight Loss Step	Second Weight Loss (%): Obs. / Cal.	No. of DMF Molecules Removed in Second Weight Loss Step
as-synthesized **1**	13.1 / 13.3	18	3.1 / 2.9	1
as-synthesized **3**	11.7 / 11.6	21	8.9 / 9.0	4
as-synthesized **4**	6 / 5.9	11	5.5/ 5.4	2.5

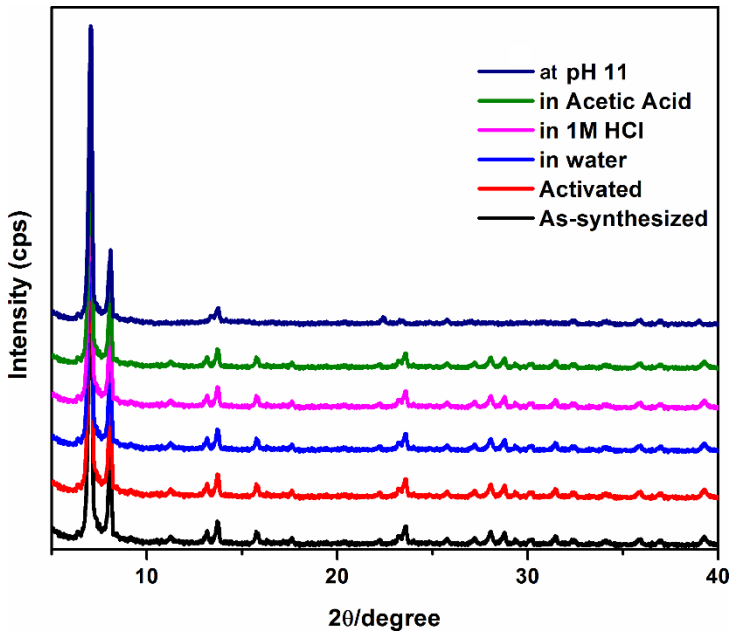

Figure S7. XRPD patterns of **1′** in different forms: as-synthesized, activated, treated with water, treated with 1M HCl and treated at pH 11.

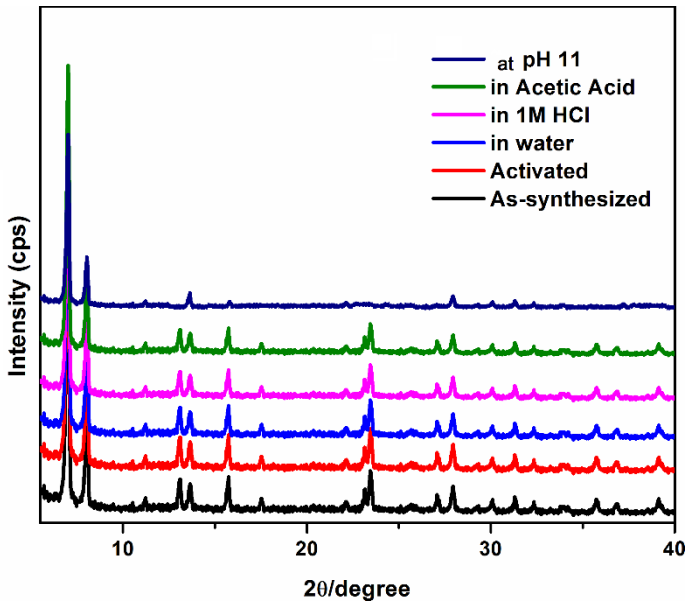

Figure S8. XRPD patterns of **3′** in different forms: as-synthesized, activated, treated with water, treated with 1M HCl and treated at pH 11.

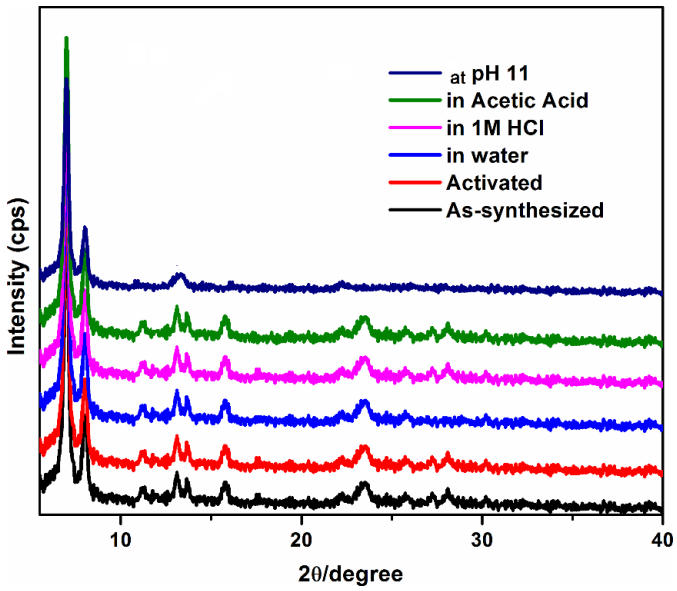

Figure S9. XRPD patterns of **4′** in different forms: as-synthesized, activated, treated with water, treated with 1M HCl and treated at pH 11.

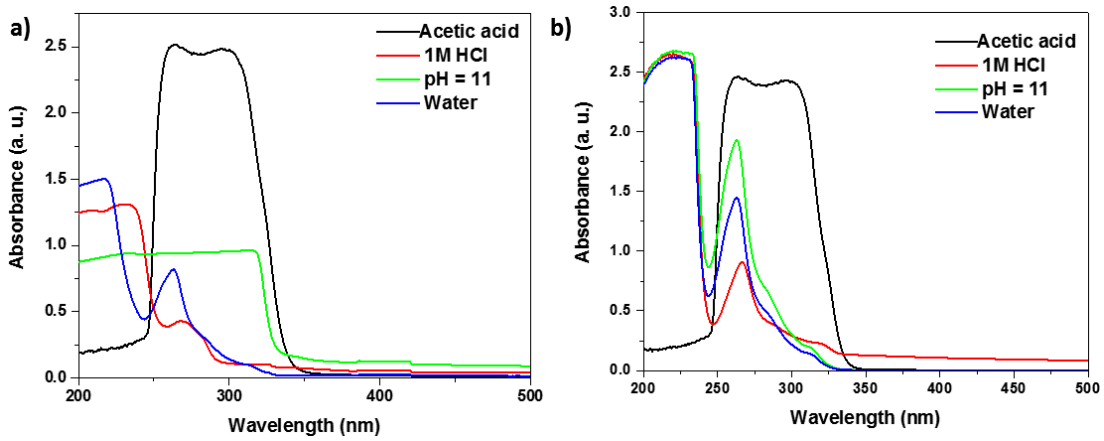

Figure S10. (a) UV-Vis spectra of the supernatants after stirring **1′** in different liquids. (b) UV-Vis spectra of free H_2TDC ligand in different liquids.

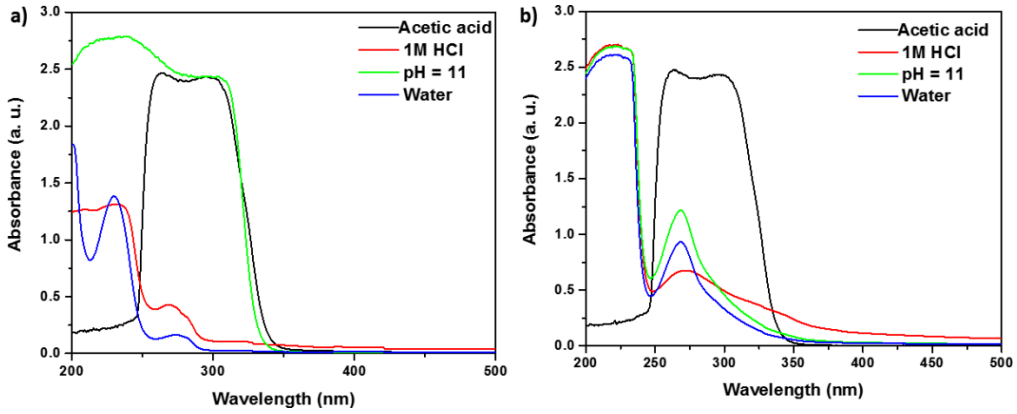

Figure S11. (a) UV-Vis spectra of the supernatants after stirring **3′** in different liquids. (b) UV-Vis spectra of free H_2MPTDC ligand in different liquids.

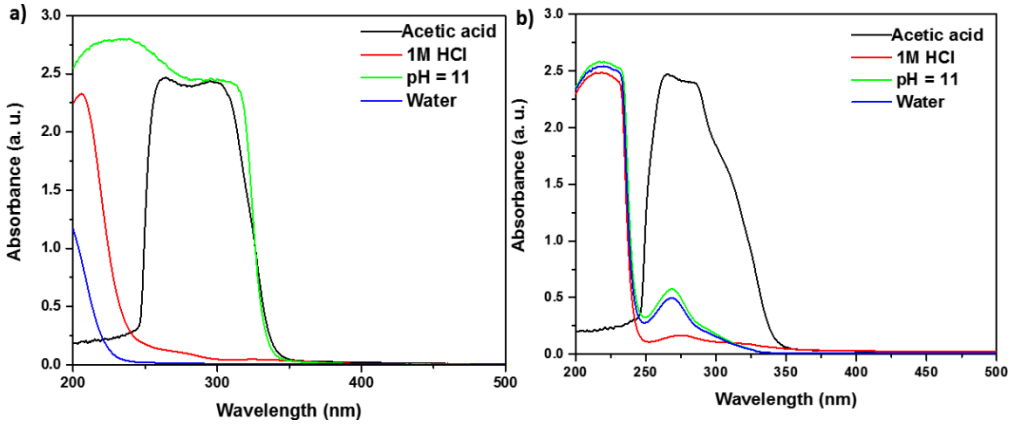

Figure S12. (a) UV-Vis spectra of the supernatants after stirring **4′** in different liquids. (b) UV-Vis spectra of free H_2DPTDC ligand in different liquids.

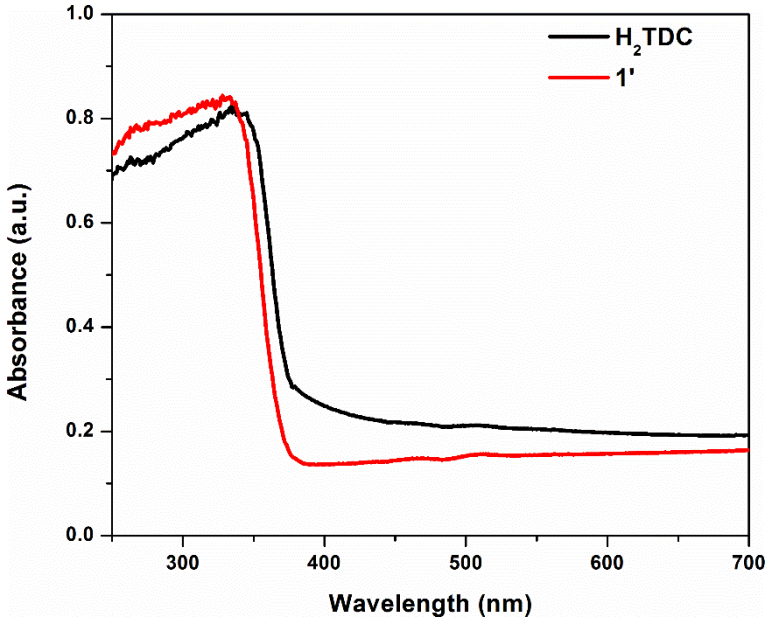

Figure S13. Diffuse reflectance UV-visible absorption spectra of H_2TDC ligand and **1′**.

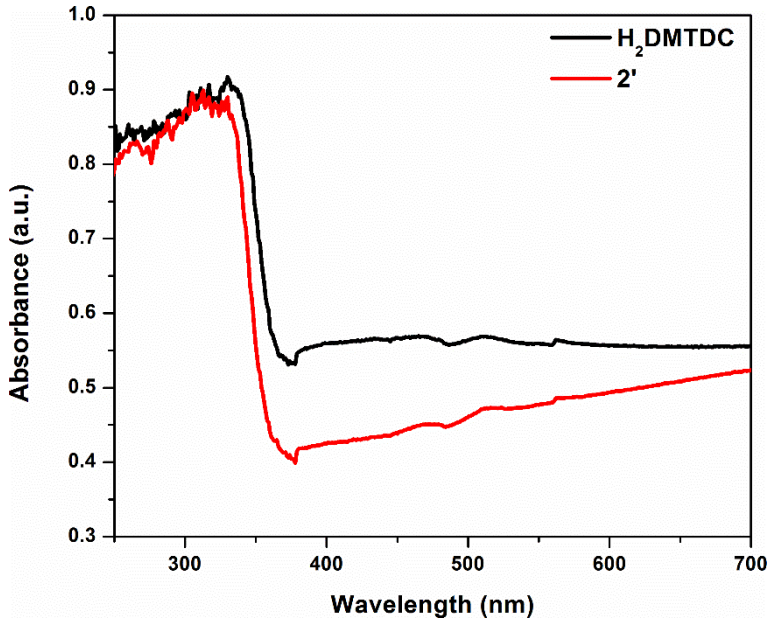

Figure S14. Diffuse reflectance UV-visible absorption spectra of H_2DMTDC ligand and **2′**.

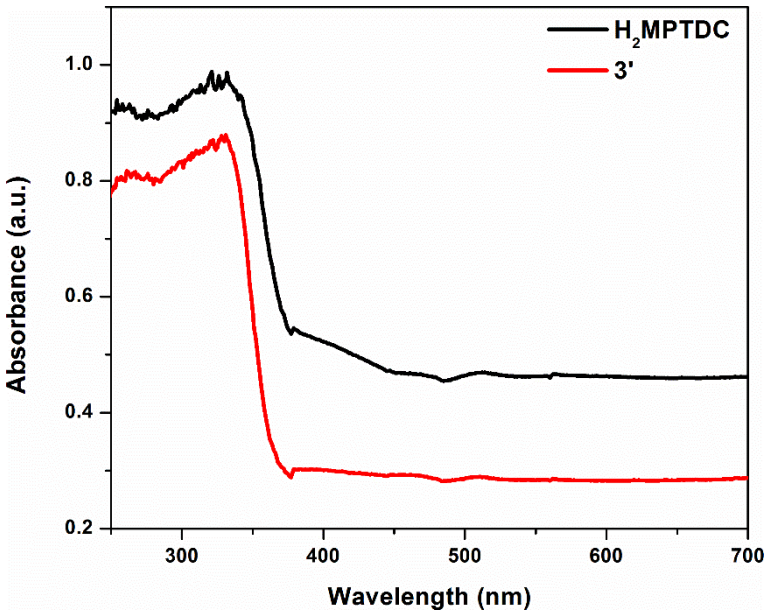

Figure S15. Diffuse reflectance UV-visible absorption spectra of H_2MPTDC ligand and **3′**.

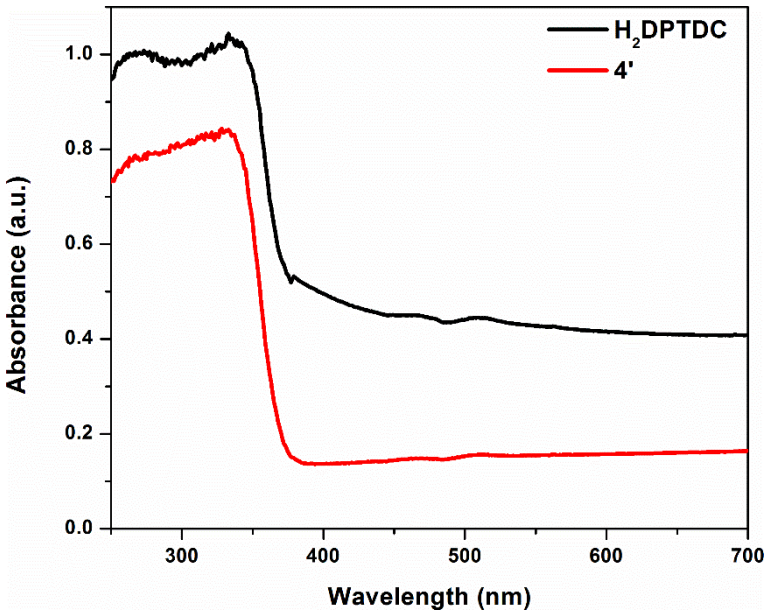

Figure S16. Diffuse reflectance UV-visible absorption spectra of H_2DPTDC ligand and **4′**.

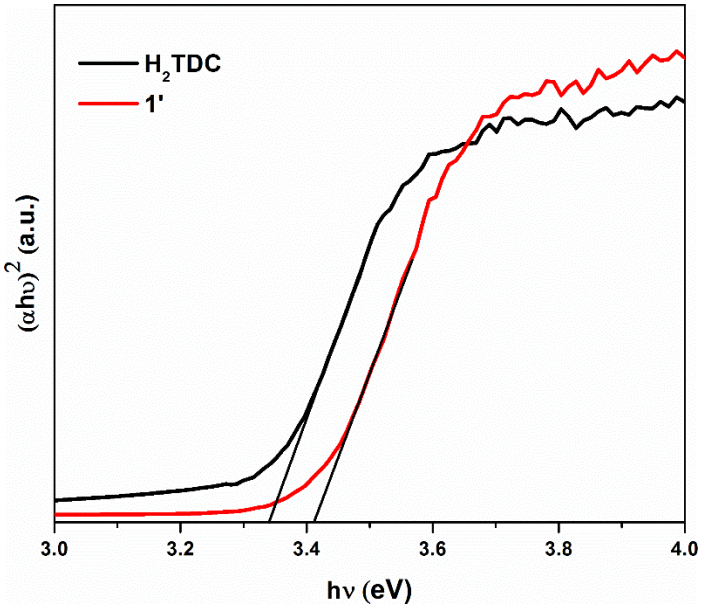

Figure S17. Tauc plot for H_2TDC ligand and **1′**.

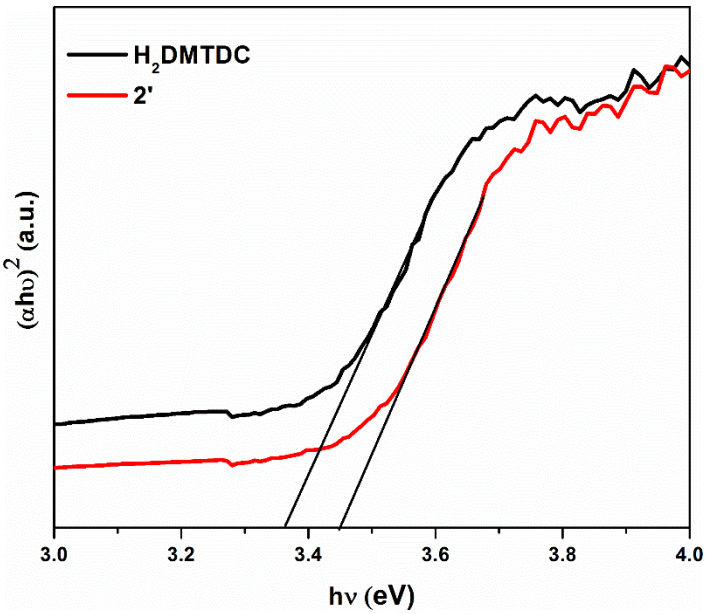

Figure S18. Tauc plot for H_2DMTDC ligand and **2′**.

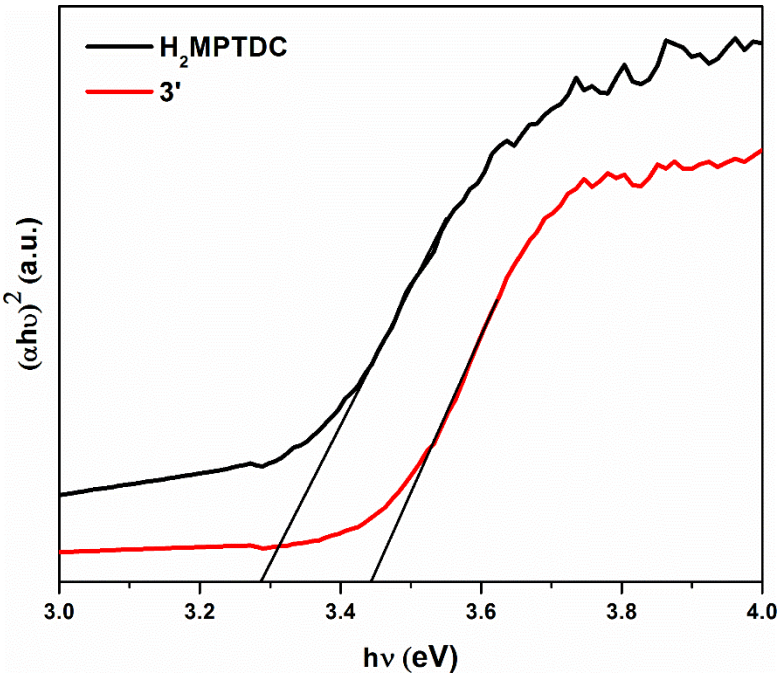

Figure S19. Tauc plot for H_2MPTDC ligand and **3′**.

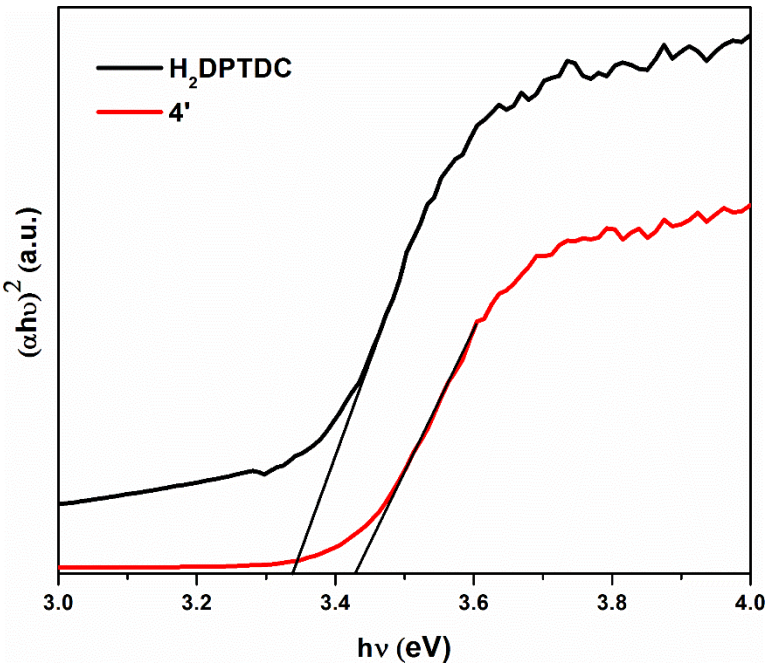

Figure S20. Tauc plot for H_2DPTDC ligand and **4′**.

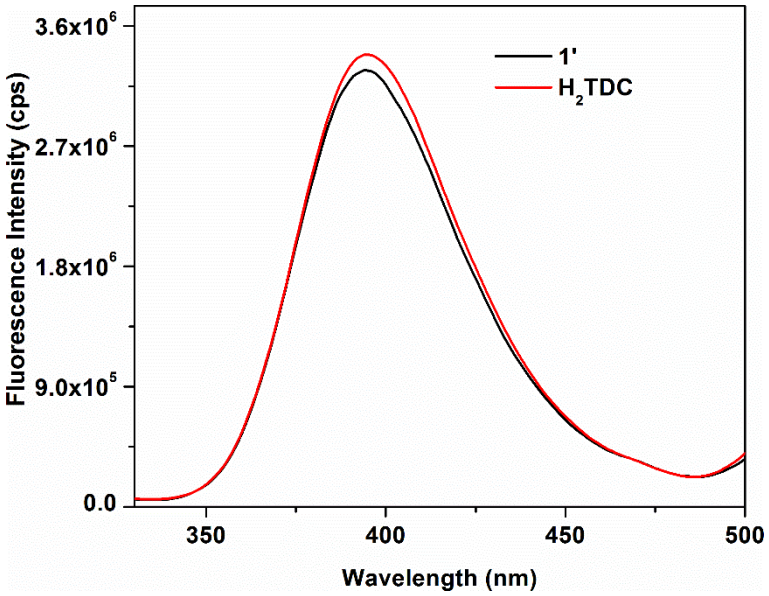

Figure S21. Solid-state fluorescence emission spectra of H_2TDC ligand and **1′** recorded at room temperature (λ_{ex} = 260 nm).

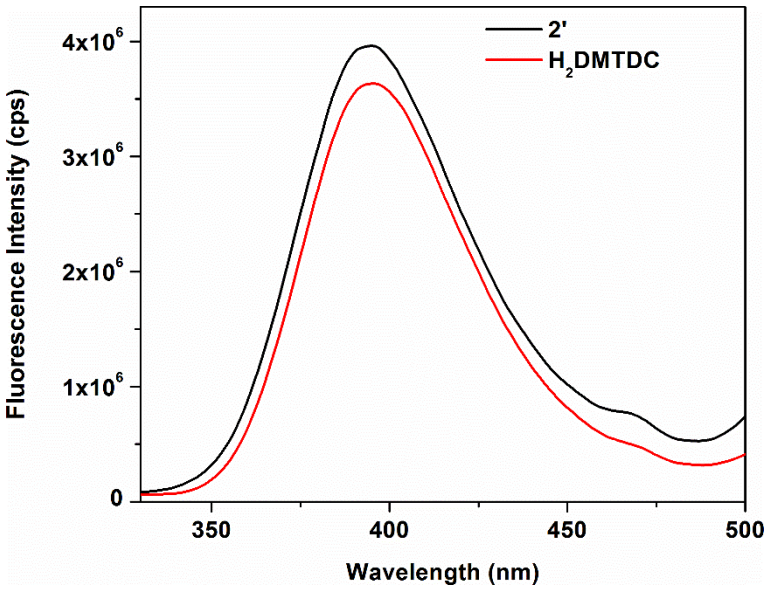

Figure S22. Solid-state fluorescence emission spectra of H_2DMTDC ligand and **2′** recorded at room temperature (λ_{ex} = 260 nm).

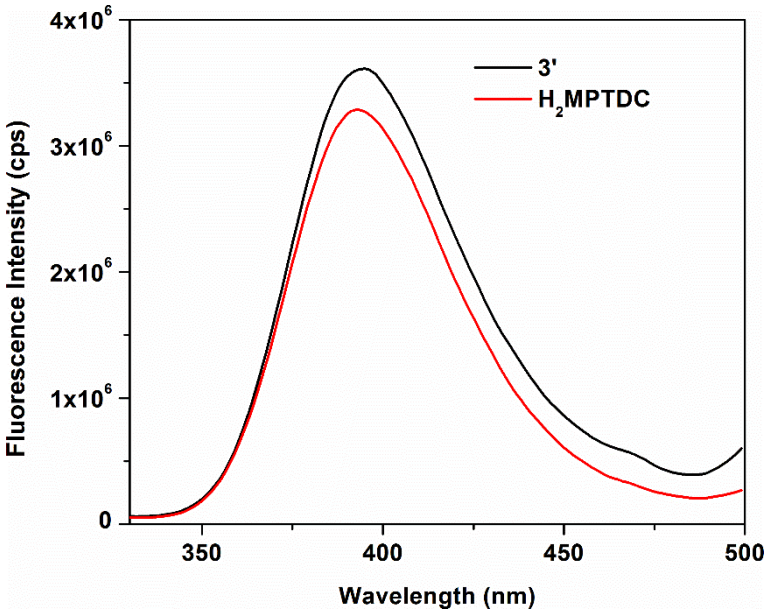

Figure S23. Solid-state fluorescence emission spectra of H_2MPTDC ligand and **3′** recorded at room temperature (λ_{ex} = 260 nm).

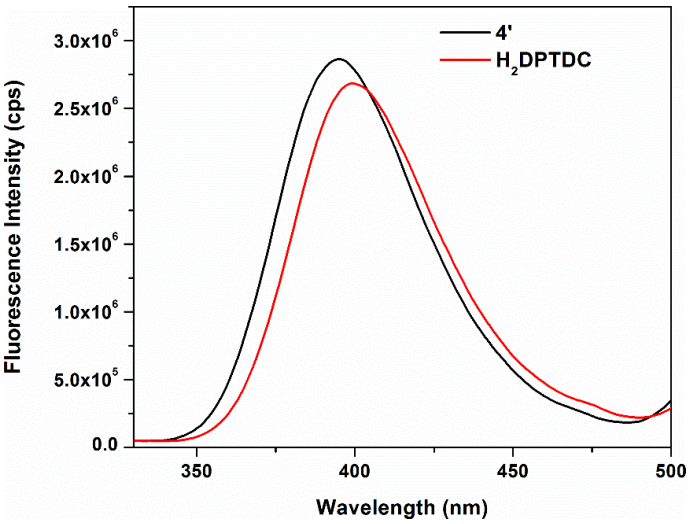

Figure S24. Solid-state fluorescence emission spectra of H_2DPTDC ligand and **4′** recorded at room temperature (λ_{ex} = 260 nm).

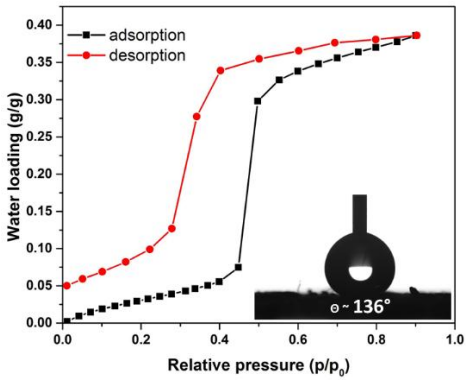

Figure S25. Water sorption isotherm of **1′** measured at 20 °C. Inset shows advancing water contact angle for **1′**.

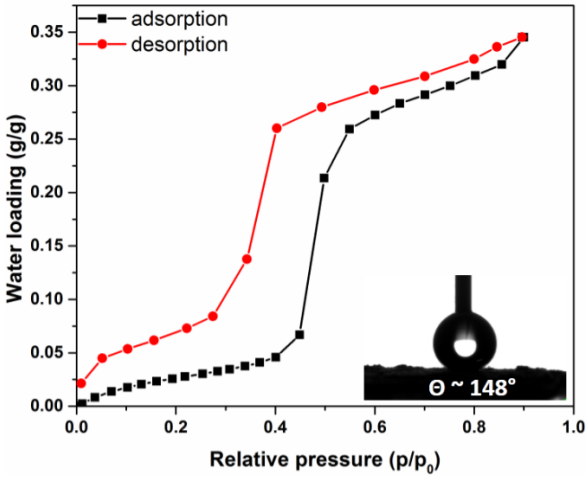

Figure S26. Water sorption isotherm of **2′** at 20 °C. Inset shows advancing water contact angle for **2′**.

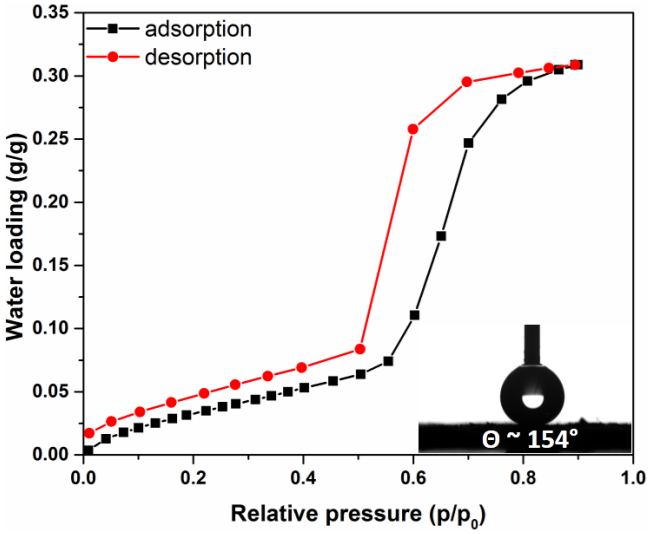

Figure S27. Water sorption isotherm of **3′** at 20 °C. Inset shows advancing water contact angle for **3′**.

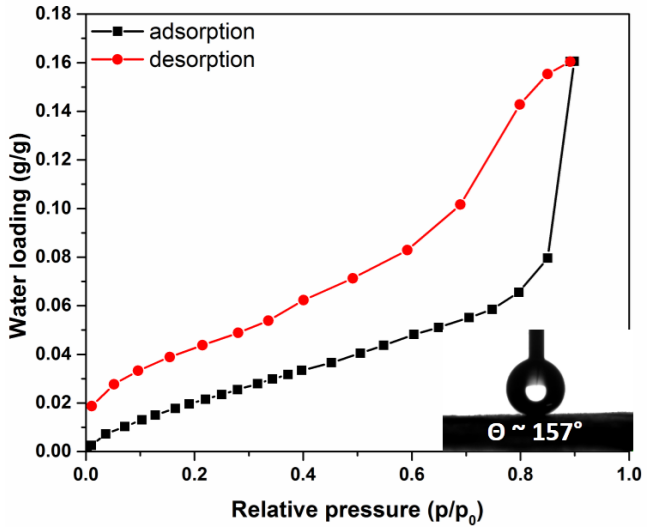

Figure S28. Water sorption isotherm of **4′** at 20°C. Inset shows advancing water contact angle for **4′**.

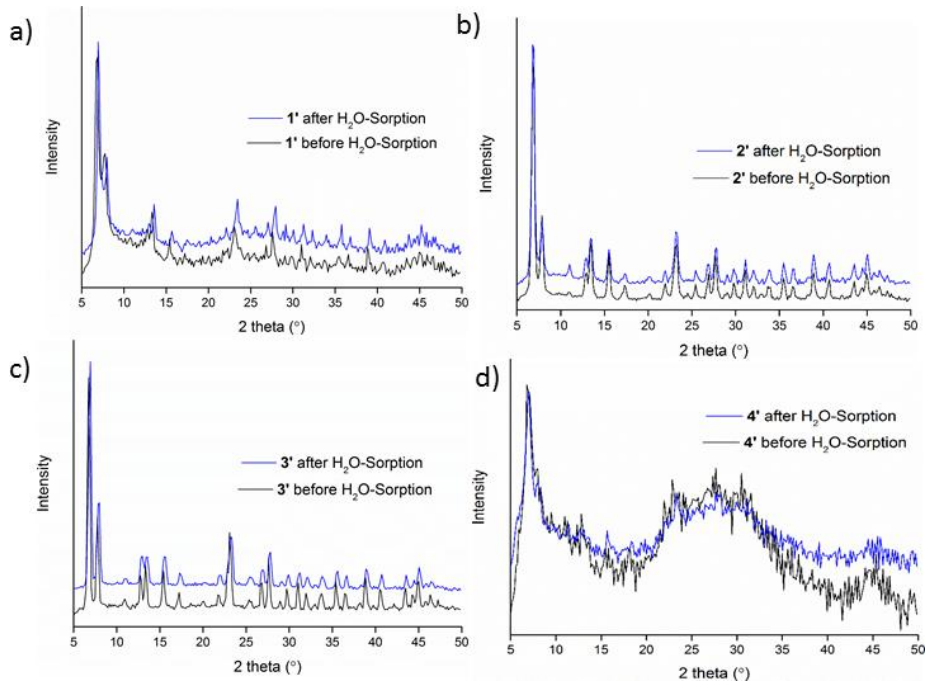

Figure S29. XRPD patterns of (a) **1′**, (b) **2′**, (c) **3′** and (d) **4′** before and after the water sorption measurements.

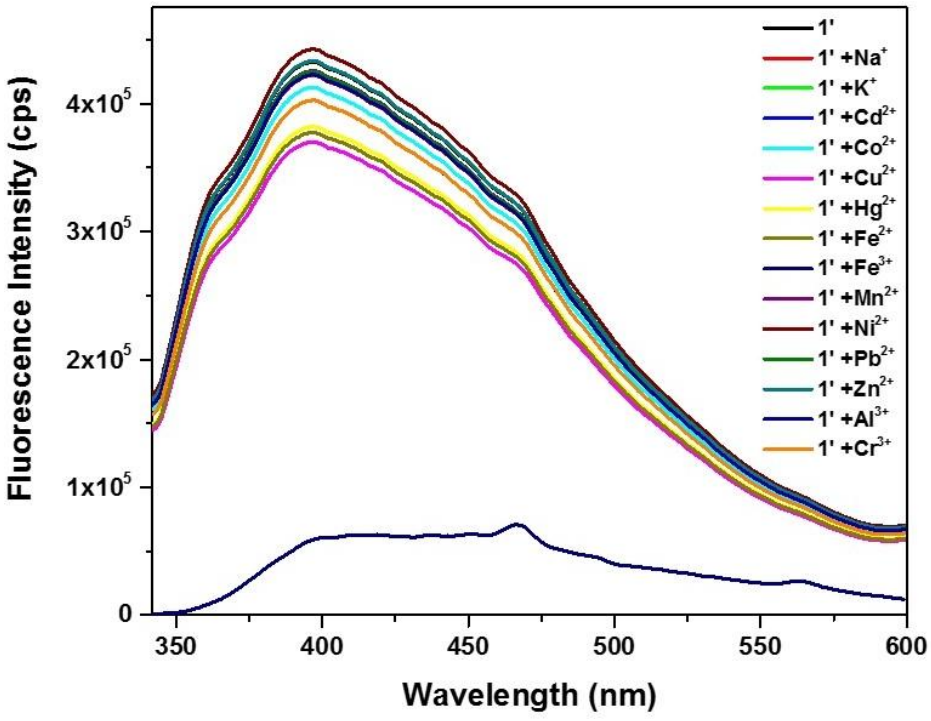

Figure S30. Change in the fluorescence intensity of **1′** upon addition of 10 mM solutions (500 µL) of different metal ions.

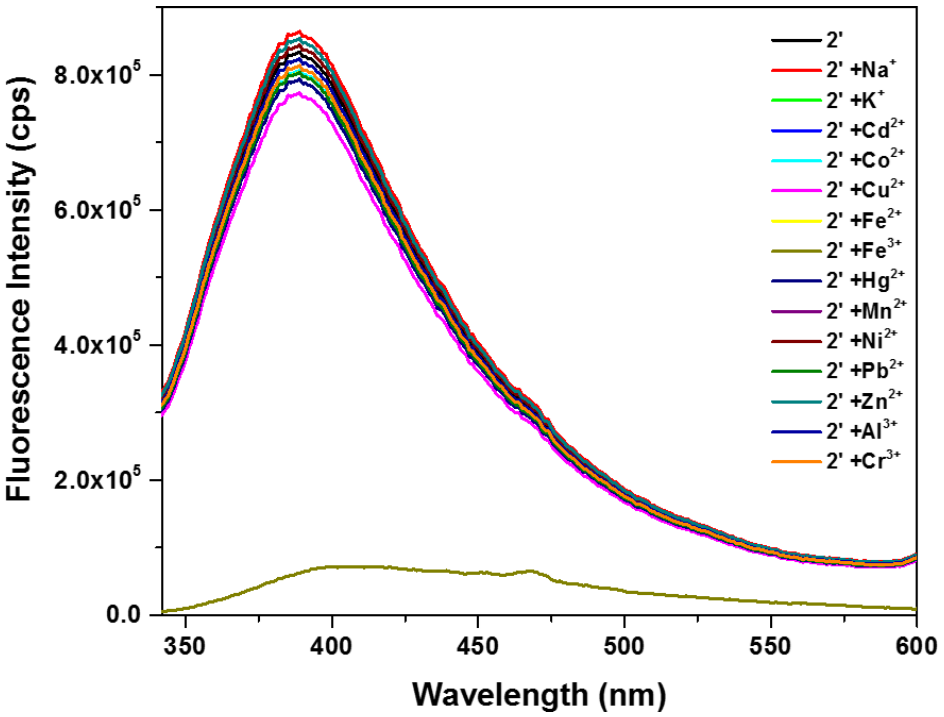

Figure S31. Change in the fluorescence intensity of **2′** upon addition of 10 mM solutions (500 µL) of different metal ions.

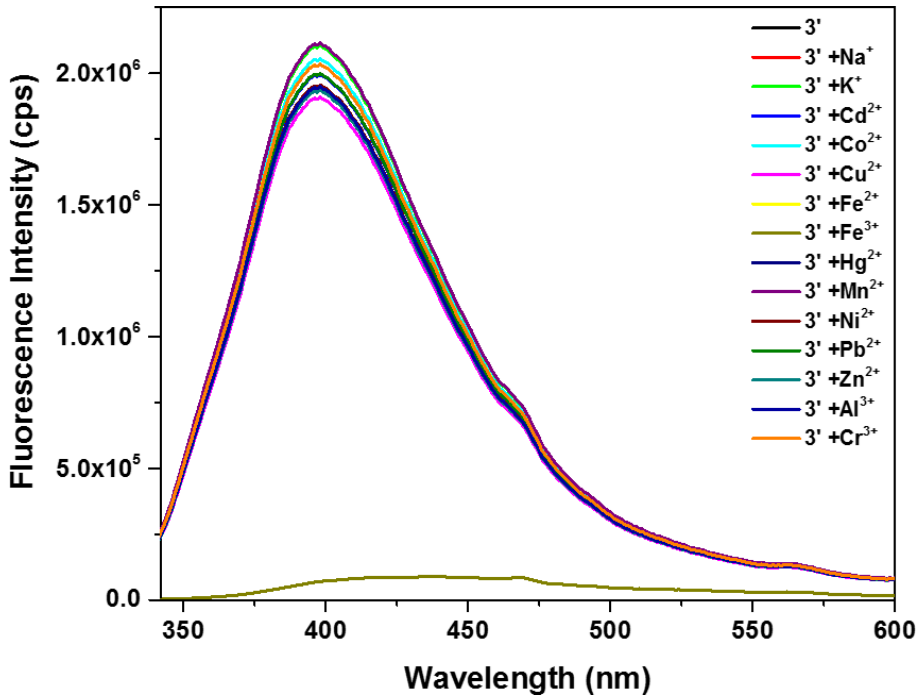

Figure S32. Change in the fluorescence intensity of **3′** upon addition of 10 mM solutions (500 µL) of different metal ions.

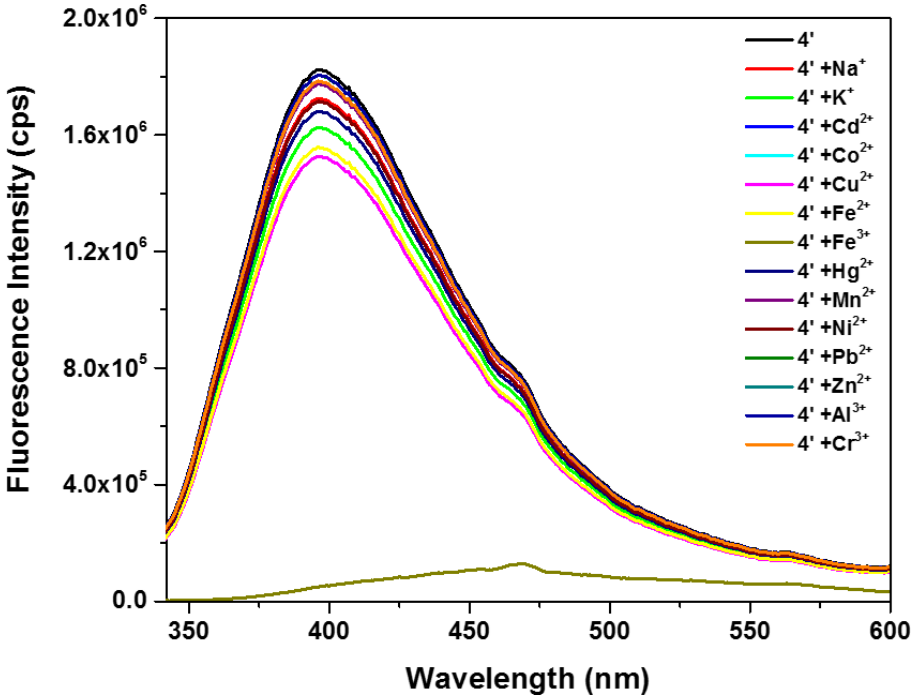

Figure S33. Change in the fluorescence intensity of **4′** upon addition of 10 mM solutions (500 µL) of different metal ions.

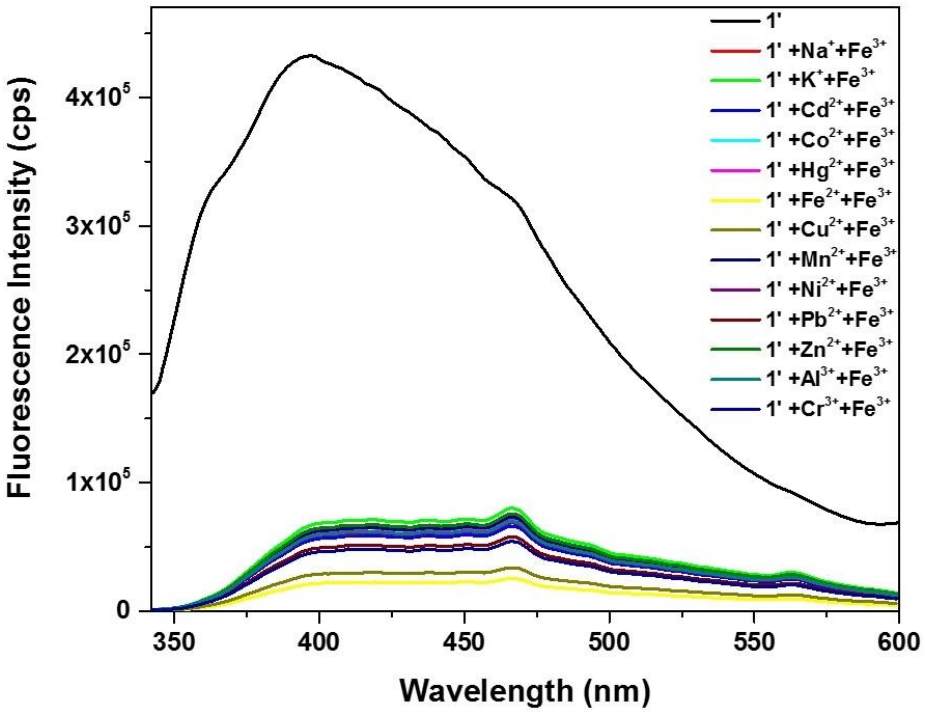

Figure S34. Change in the fluorescence intensity of **1′** upon addition of 10 mM solutions (500 µL) of different metal ions in presence of Fe^{3+} ion.

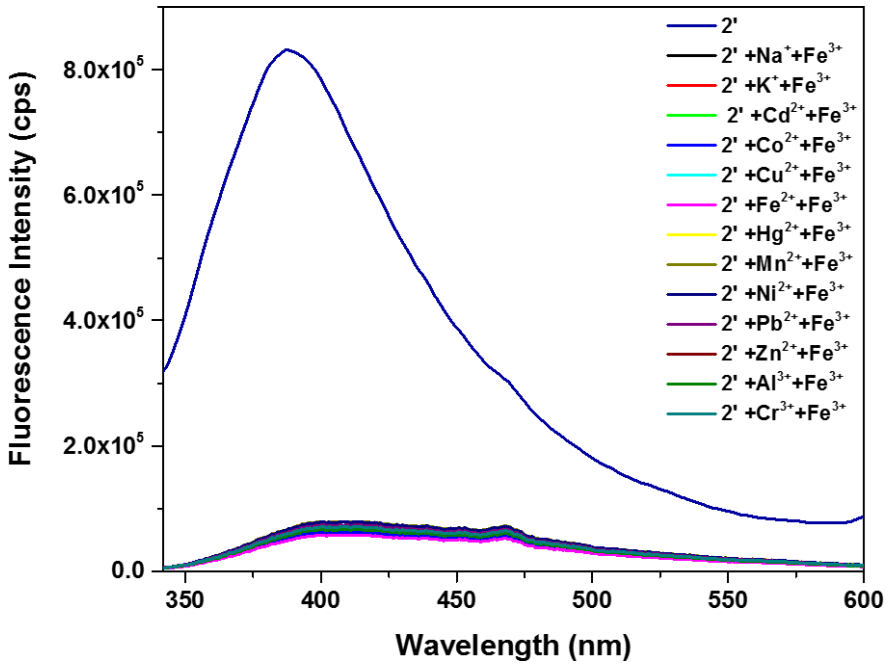

Figure S35. Change in the fluorescence intensity of **2′** upon addition of 10 mM solutions (500 µL) of different metal ions in presence of Fe^{3+} ion.

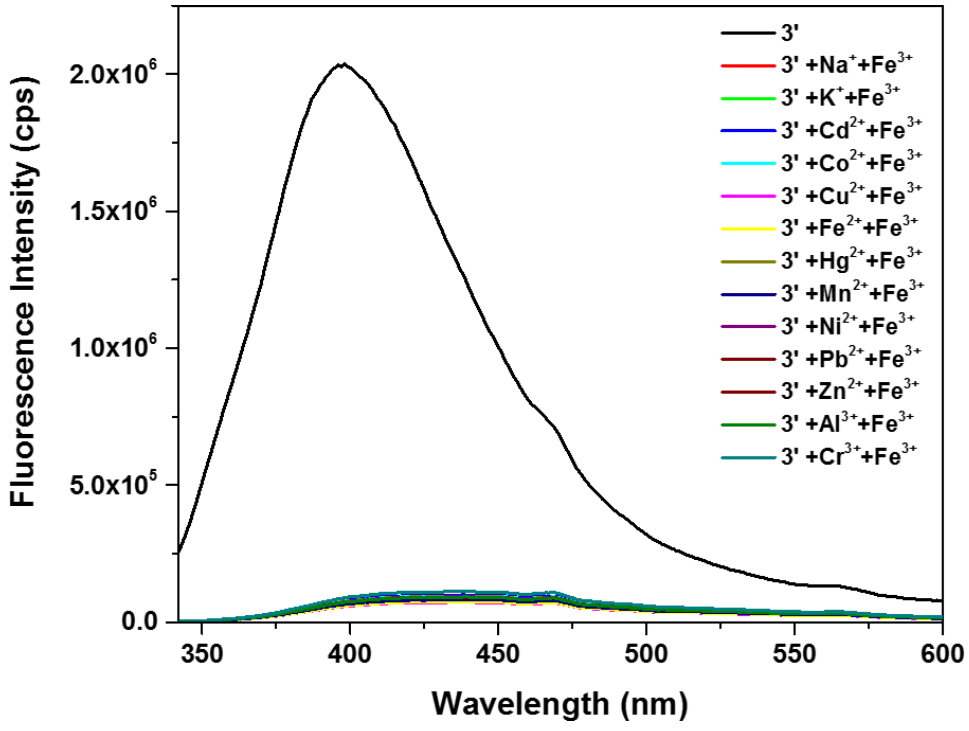

Figure S36. Change in the fluorescence intensity of **3′** upon addition of 10 mM solutions (500 µL) of different metal ions in presence of Fe^{3+} ion.

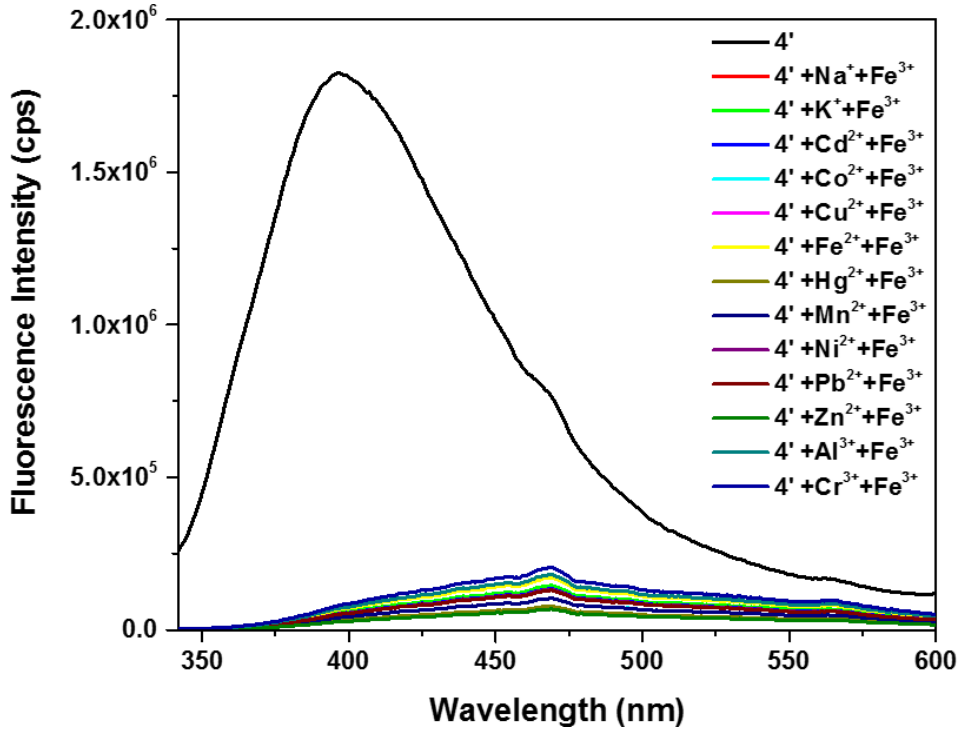

Figure S37. Change in the fluorescence intensity of **4′** upon addition of 10 mM solutions (500 µL) of different metal ions in presence of Fe^{3+} ion.

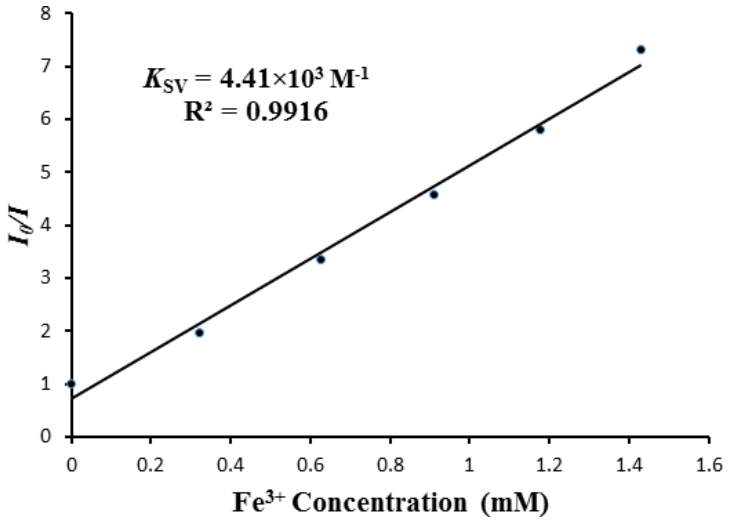

Figure S38. Stern-Volmer plot for the fluorescence quenching of **1′** in presence of Fe^{3+} in aqueous solution.

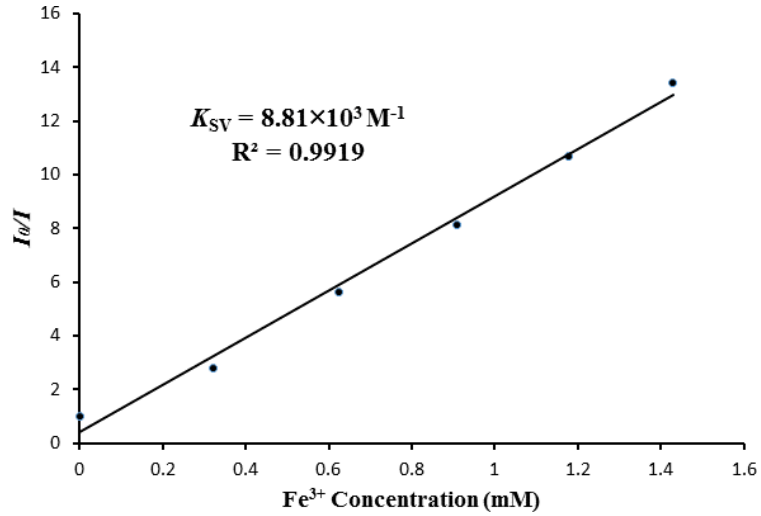

Figure S39. Stern-Volmer plot for the fluorescence quenching of **2′** in presence of Fe^{3+} in aqueous solution.

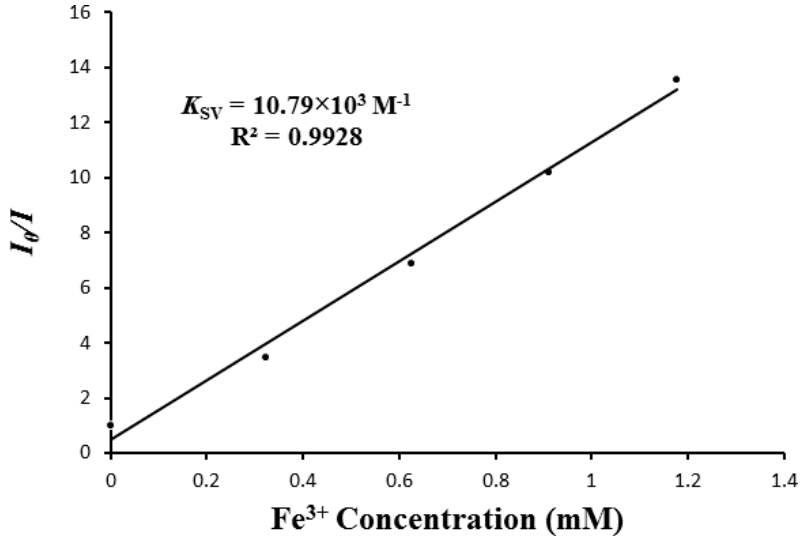

Figure S40. Stern-Volmer plot for the fluorescence quenching of **3′** in presence of Fe^{3+} in aqueous solution.

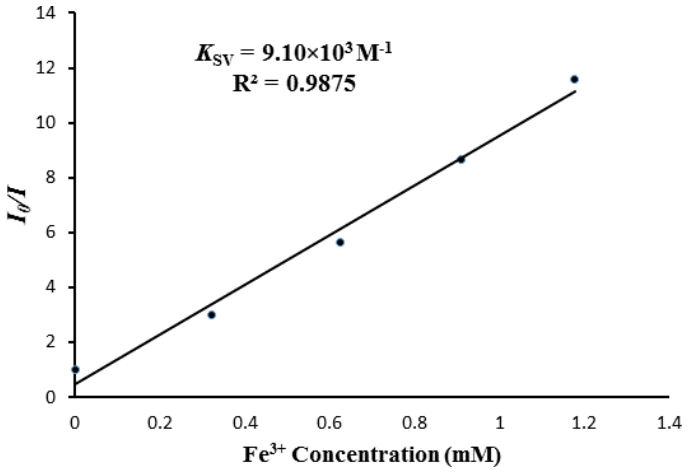

Figure S41. Stern-Volmer plot for the fluorescence quenching of **4′** in presence of Fe^{3+} in aqueous solution.

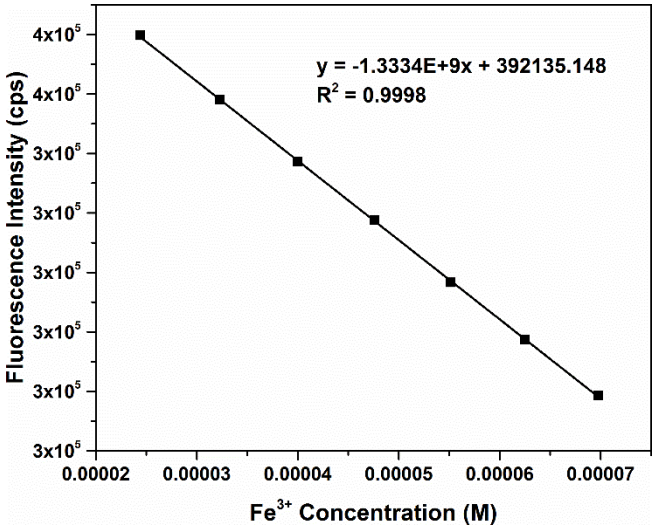

Figure S42. Change in the fluorescence intensity of **1′** in aqueous solution as a function of Fe^{3+} concentration.

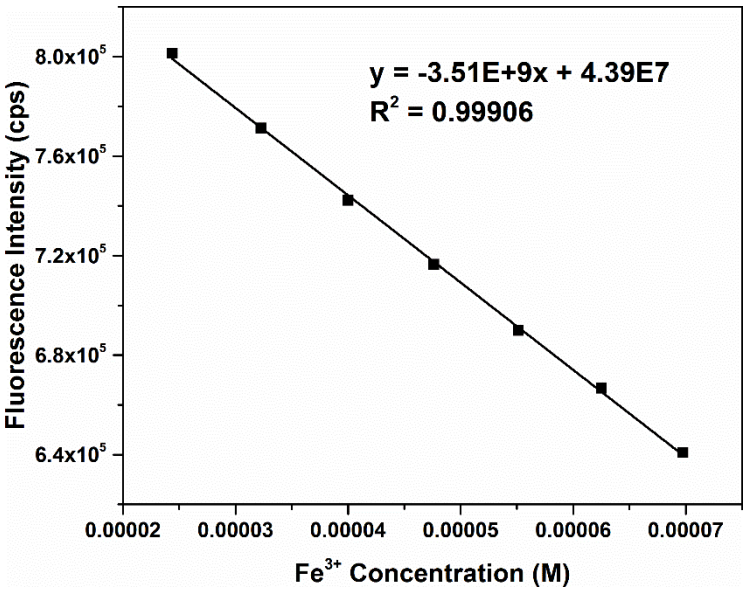

Figure S43. Change in the fluorescence intensity of **2′** in aqueous solution as a function of Fe^{3+} concentration.

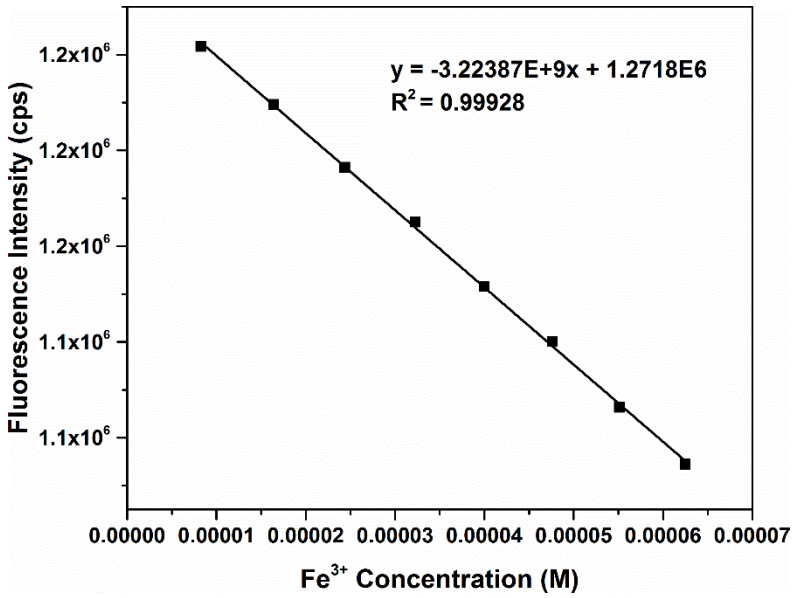

Figure S44. Change in the fluorescence intensity of **3′** in aqueous solution as a function of Fe^{3+} concentration.

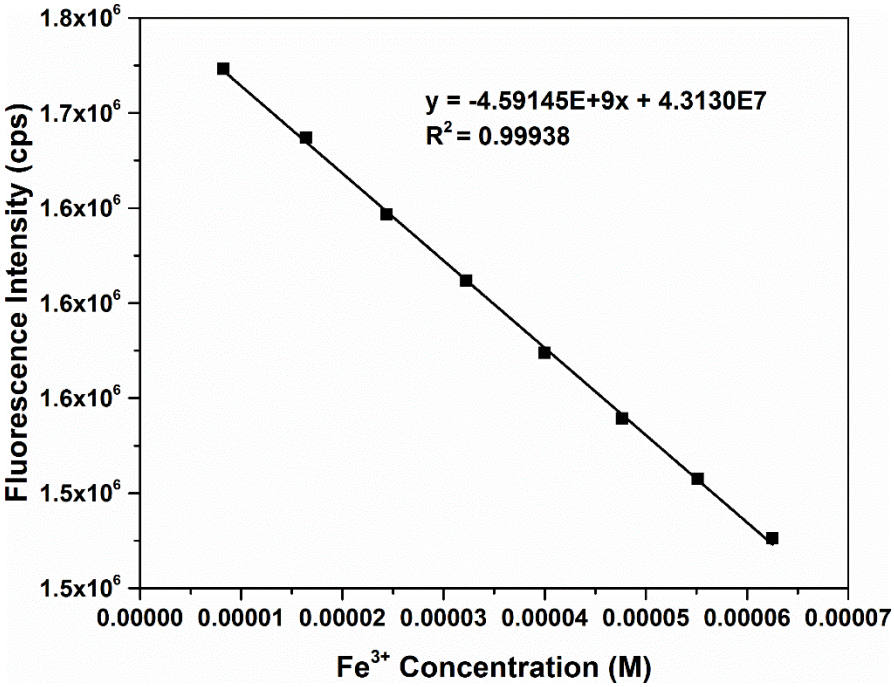

Figure S45. Change in the fluorescence intensity of **4′** in aqueous solution as a function of Fe^{3+} concentration.

Table S3. A comparison of the Stern-Volmer constant (K_{sv}), detection limit and medium used for Fe^{3+} detection for MOFs reported till date.

Sl. No.	MOF	K_{sv} ($\times 10^4$ M^{-1})	Detection Limit	Medium Used	Ref.
1	$[Zr_6O_4(OH)_4(C_8H_2O_4S_2)_6]\cdot DMF\cdot 18H_2O$	0.44	1.26×10^{-6} M	Water	This work
2	$[Zr_6O_4(OH)_4(C_{10}H_6O_4S_2)_6]\cdot 4.8DMF\cdot 10H_2O$	0.88	8.57×10^{-7} M	Water	This work
3	$[Zr_6O_4(OH)_4\ (C_{15}H_8O_4S_2)_6]\cdot 4DMF\cdot 21H_2O$	1.07	9.33×10^{-7} M	Water	This work
4	$[Zr_6O_4(OH)_4\ (C_{20}H_{10}O_4S_2)_6]\cdot 2.5DMF\cdot 11H_2O$	0.91	3.4×10^{-7} M	Water	This work
6	$[La(TPT)(DMSO)_2]\cdot H_2O$	1.36	-	Ethanol	[3]
7	$[H(H_2O)_8][DyZn_4(imdc)_4(im)_4]$	2.88	-	DMSO	[4]
8	EuL_3	0.41	10^{-4} M	Ethanol	[5]
9	$[Eu_2(MFDA)_2(HCOO)_2(H_2O)_6]\cdot H_2O$	-	3.3×10^{-7} M	DMF	[6]

10	$[Cd(H_2L_a)_{0.5}(H_2L_b)_{0.5}(H_2O)]$	-	10^{-5} M	Water	[7]
11	$[(CH_3)_2NH_2]\cdot[Tb(bptc)]\cdot x$solvents	-	72.76 ppm	Ethanol	[8]
12	$[Ln_2(Ccbp)_3\cdot 6H_2O]\cdot 3Cl^-\cdot 4H_2O$	11.43	-	Ethanol	[9]
13	Eu^{3+}@MIL-124	3.87	0.28×10^{-6} M	Water	[10]
14	MIL-53(Al)	-	0.9×10^{-6} M	PBS buffer	[11]
15	$[Ln(Hpzbc)_2(NO_3)]\cdot H_2O$	-	2.6×10^{-5} M	Ethanol	[12]
16	$[Tb(BTB)(DMF)]\cdot 1.5DMF\cdot 2.5H_2O$	-	10^{-5} M	Ethanol	[13]
17	$[Tb_4(OH)_4(DSOA)_2(H_2O)_8]\cdot(H_2O)_8$	3.5	-	Water	[14]
18	Tb^{3+}@Cd-MOF	11.08	0.010 mM	DMF	[15]

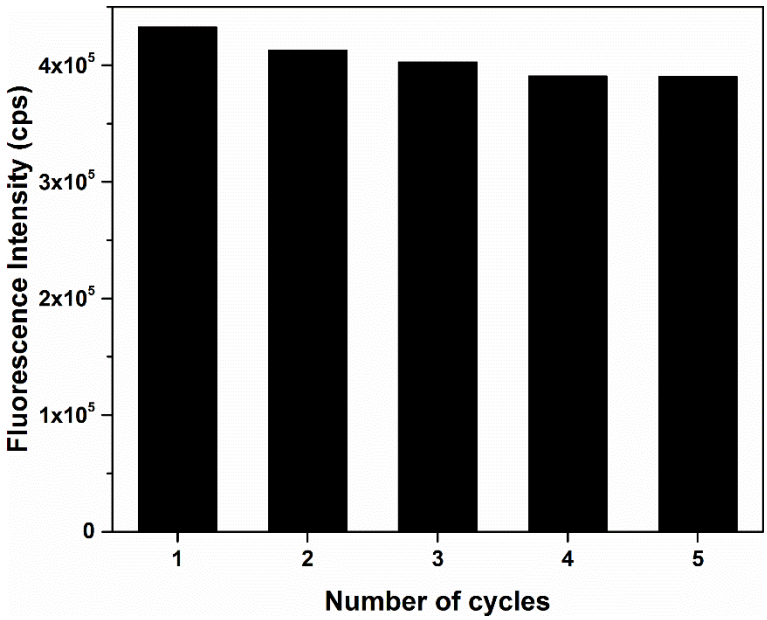

Figure S46. Reproducibility of the quenching efficiency of the aqueous suspension of **1′** in aqueous solution towards 10 mM Fe^{3+} solution.

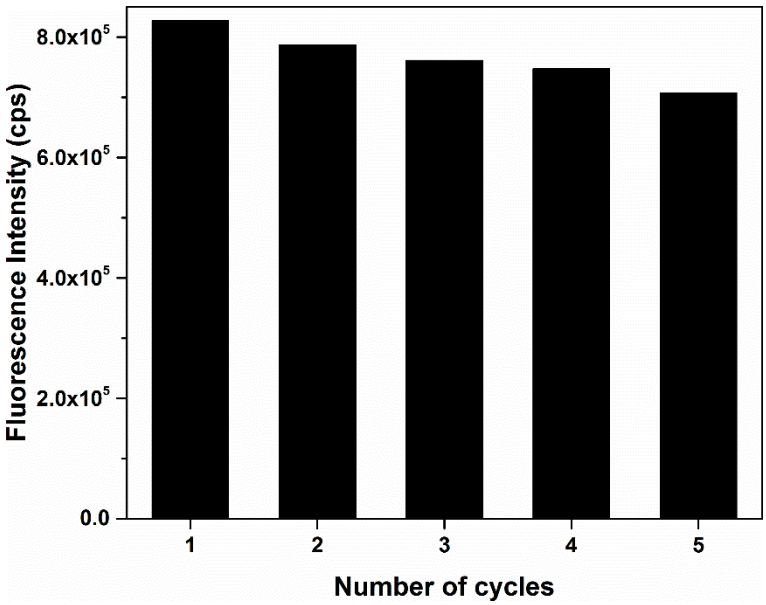

Figure S47. Reproducibility of the quenching efficiency of the aqueous suspension of **2′** in aqueous solution towards 10 mM Fe^{3+} solution.

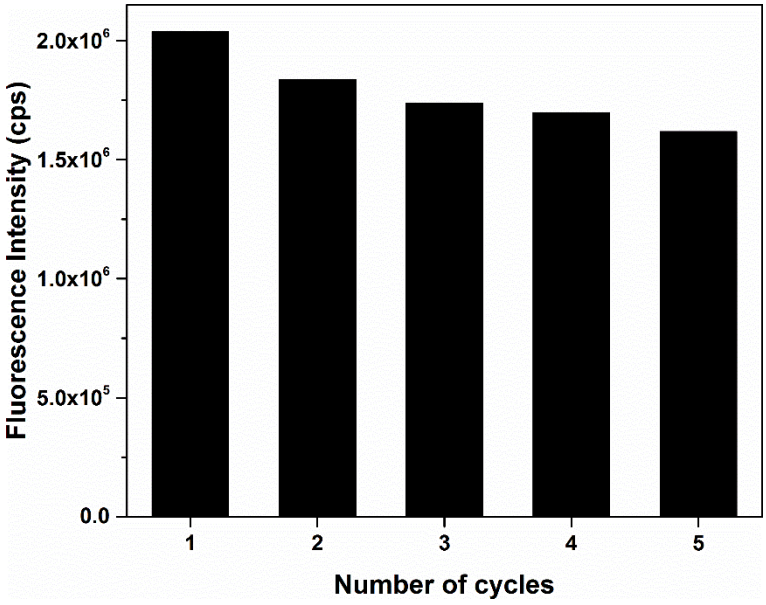

Figure S48. Reproducibility of the quenching efficiency of the aqueous suspension of **3′** in aqueous solution towards 10 mM Fe^{3+} solution.

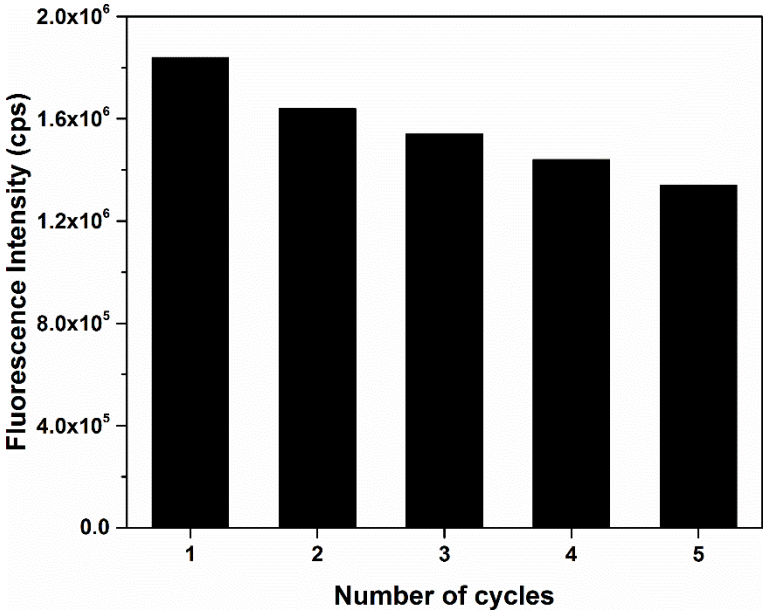

Figure S49. Reproducibility of the quenching efficiency of the aqueous suspension of **4′** in aqueous solution towards 10 mM Fe^{3+} solution.

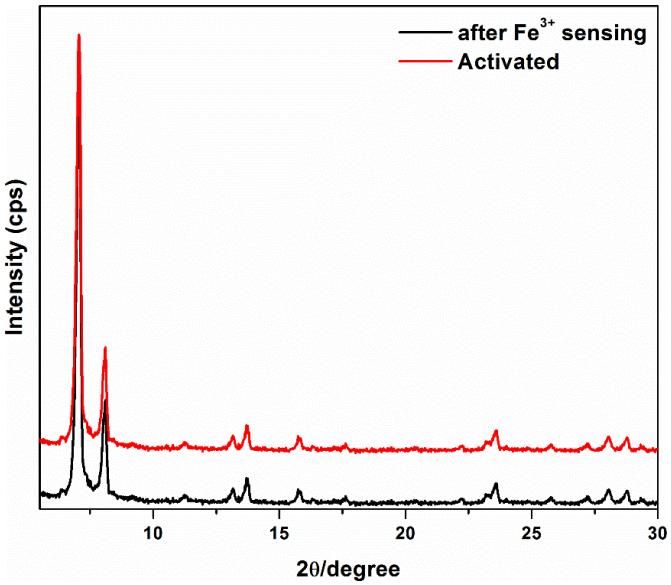

Figure S50. XRPD patterns of **1′** before and after the Fe^{3+} sensing experiment.

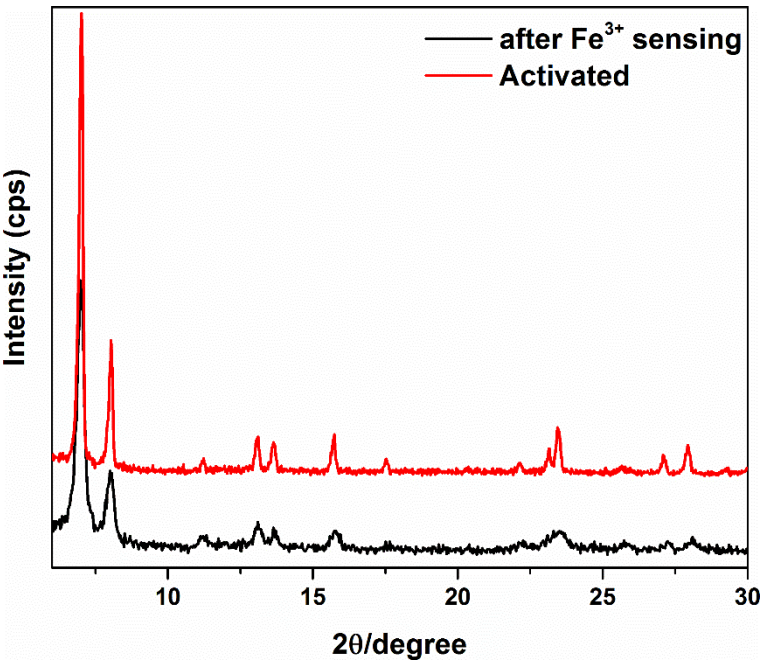

Figure S51. XRPD patterns of **2′** before and after the Fe^{3+} sensing experiment.

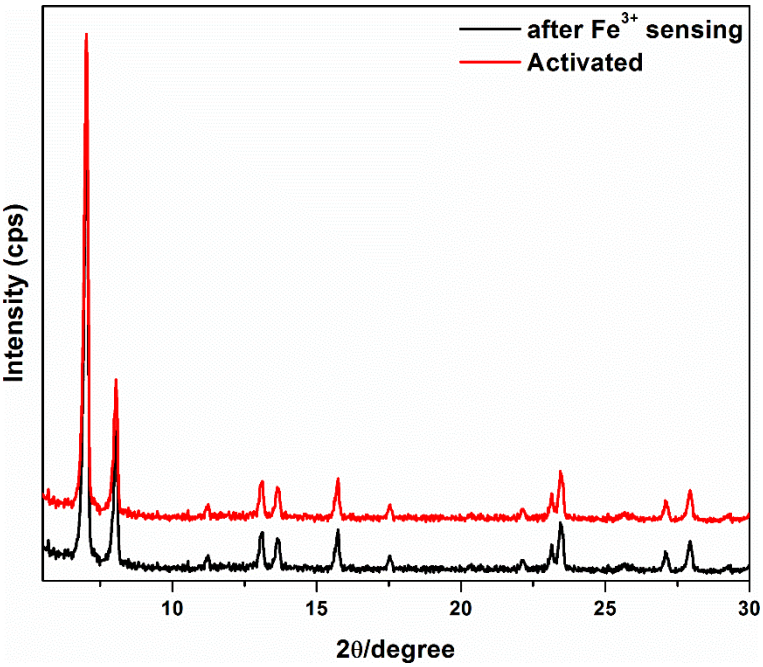

Figure S52. XRPD patterns of **3′** before and after the Fe^{3+} sensing experiment.

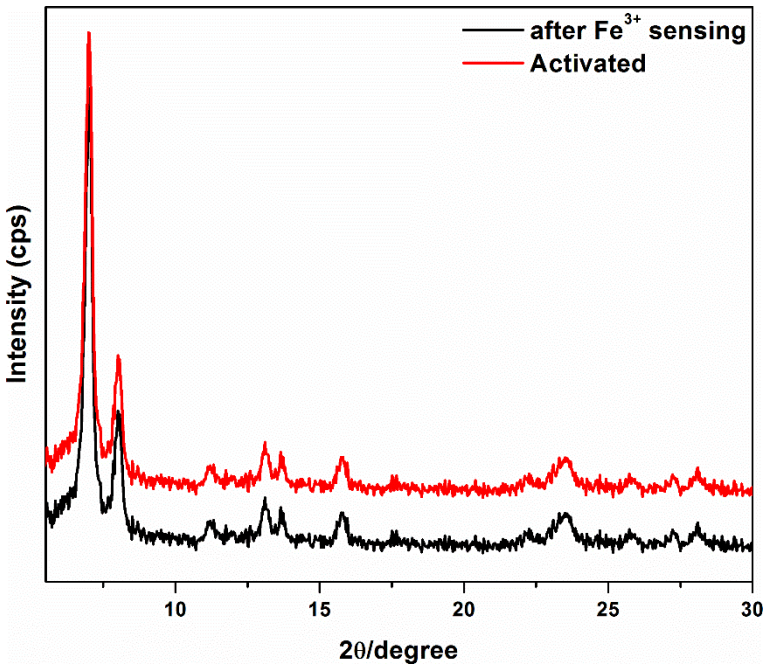

Figure S53. XRPD patterns of **4′** before and after the Fe^{3+} sensing experiment.

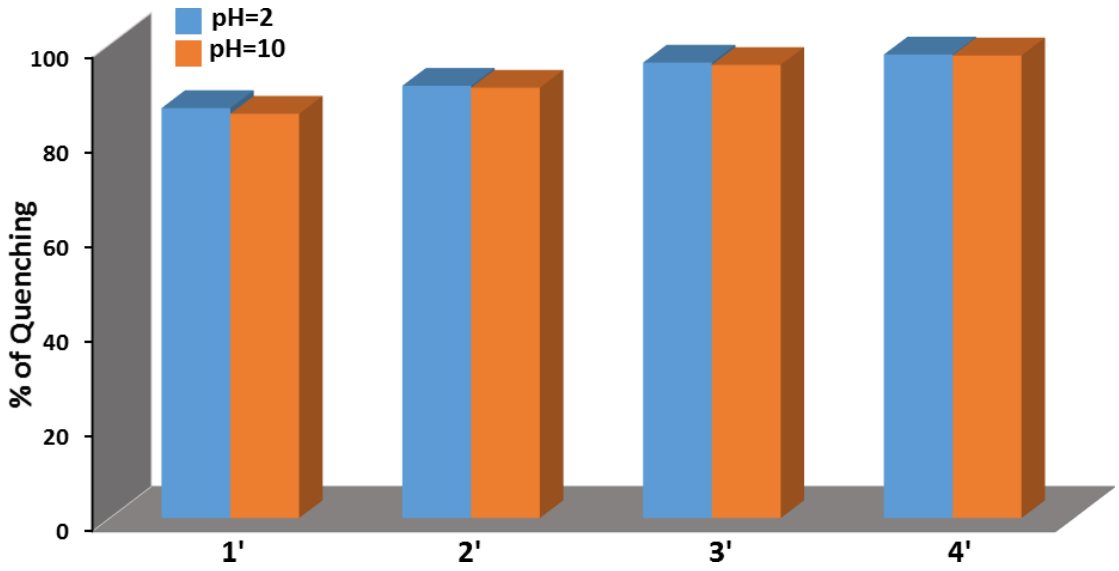

Figure S54. Effect of pH on fluorescence quenching.

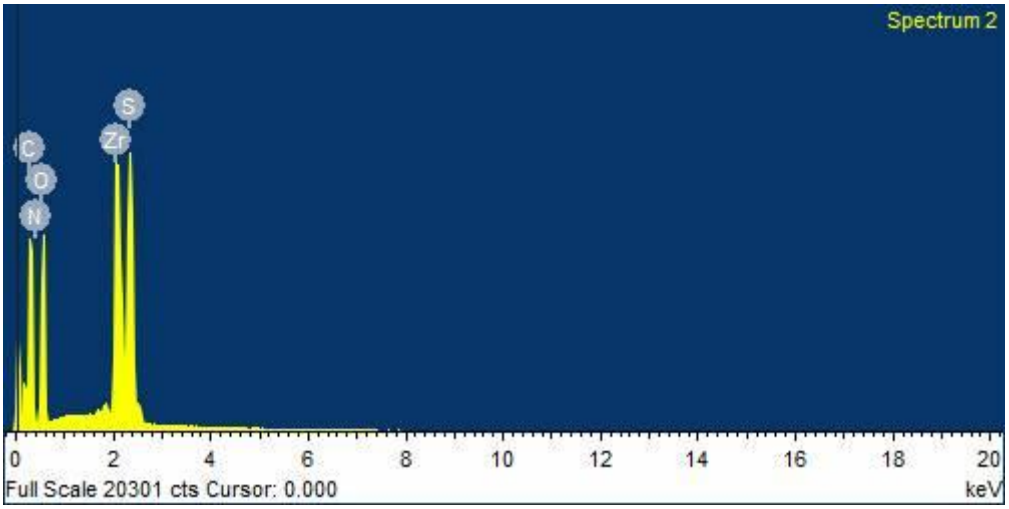

Figure 55. EDX spectrum of **1′** recovered after the Fe^{3+} sensing experiment.

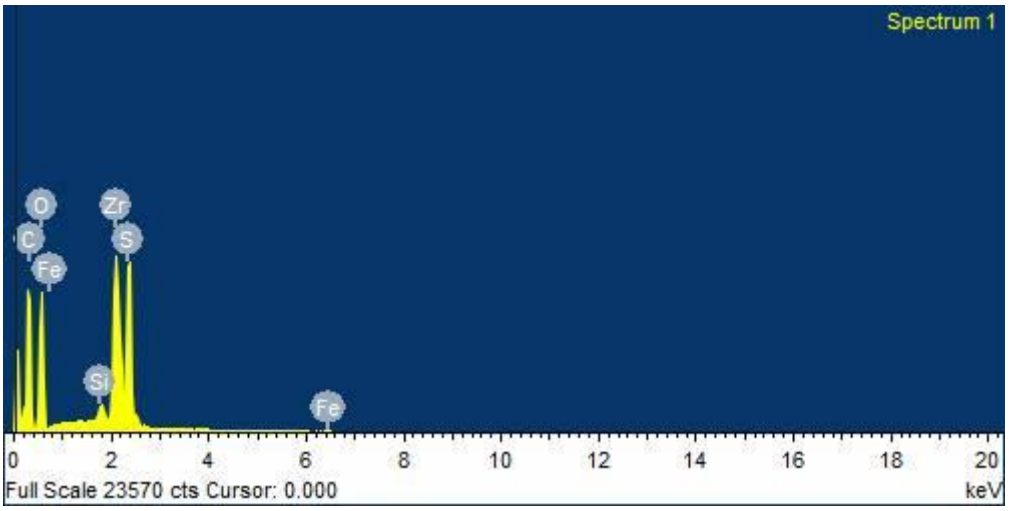

Figure S56. EDX spectrum of **2′** recovered after the Fe^{3+} sensing experiment.

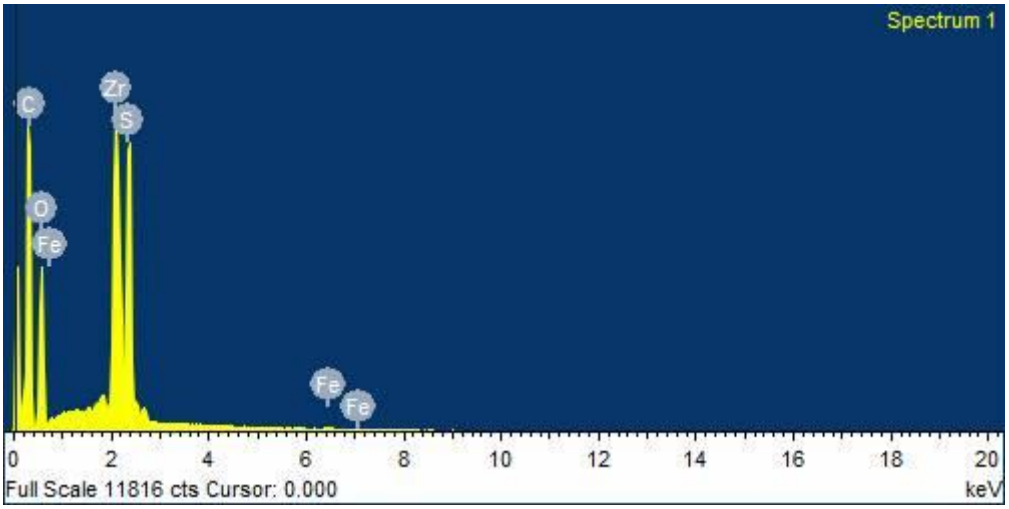

Figure S57. EDX spectrum of **3′** recovered after the Fe^{3+} sensing experiment.

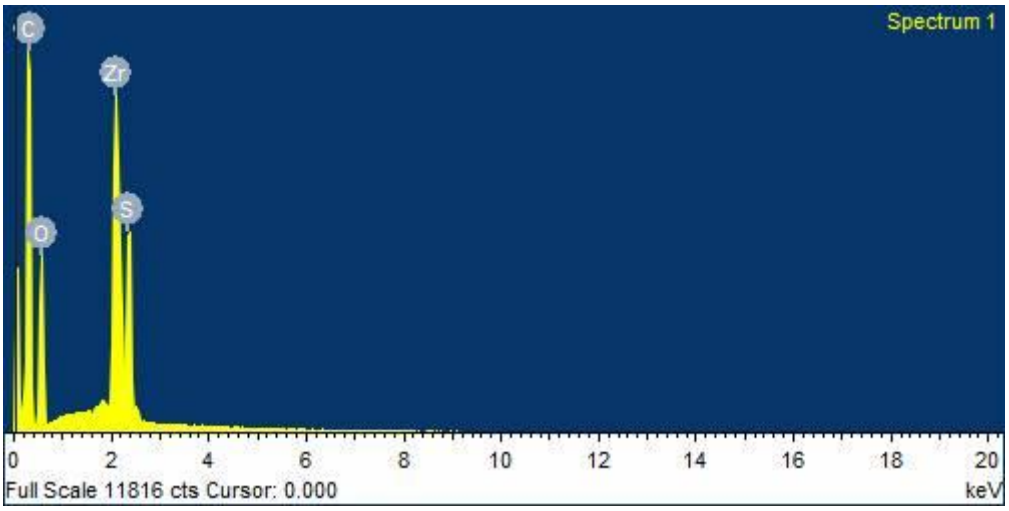

Figure S58. EDX spectrum of **4′** recovered after the Fe^{3+} sensing experiment.

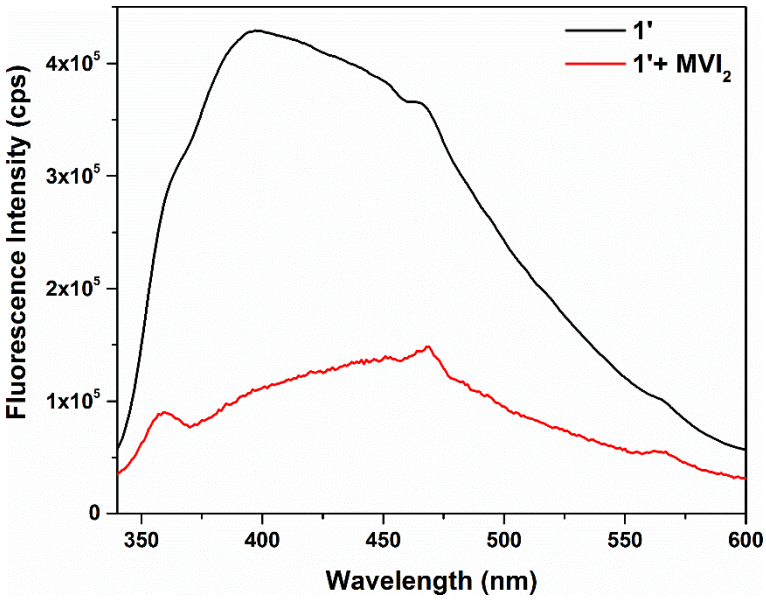

Figure S59. Change in the fluorescence intensity of **1′** in presence of 10 mM MVI_2 (500 µL).

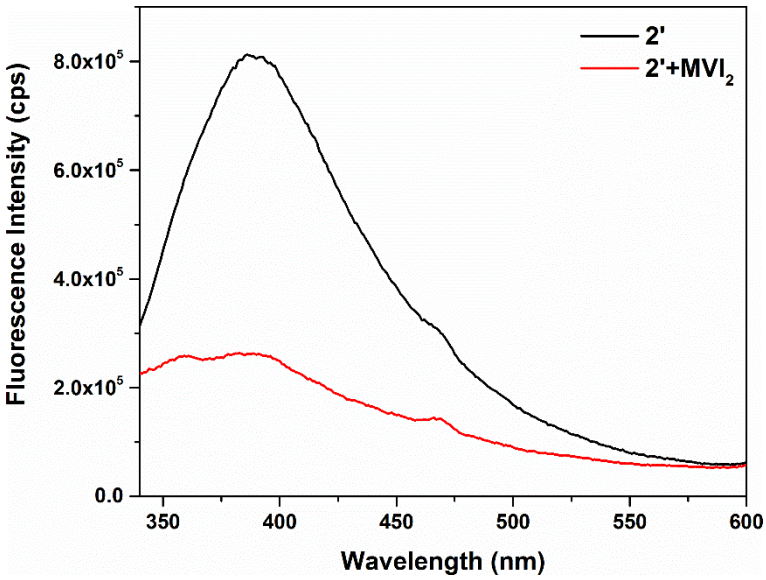

Figure S60. Change in the fluorescence intensity of **2′** in presence of 10 mM MVI_2 (500 µL).

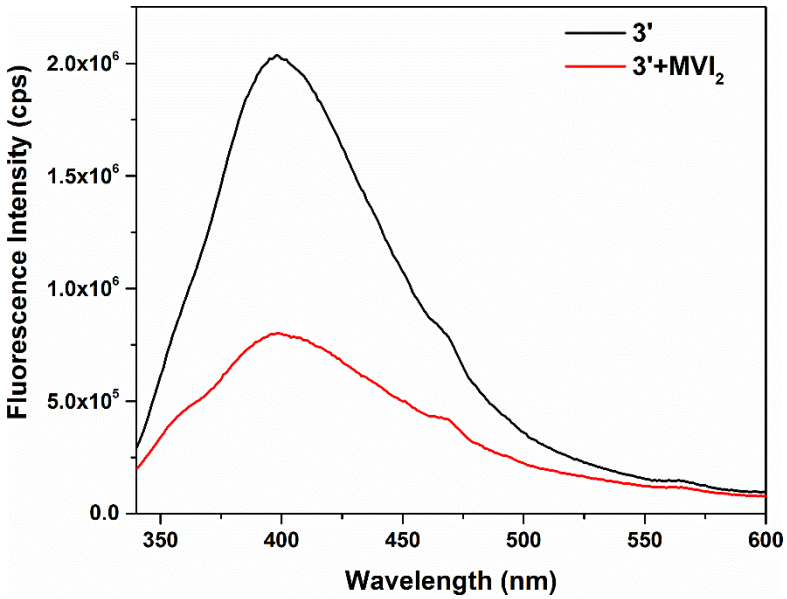

Figure S61. Change in the fluorescence intensity of **3′** in presence of 10 mM MVI_2 (500 µL).

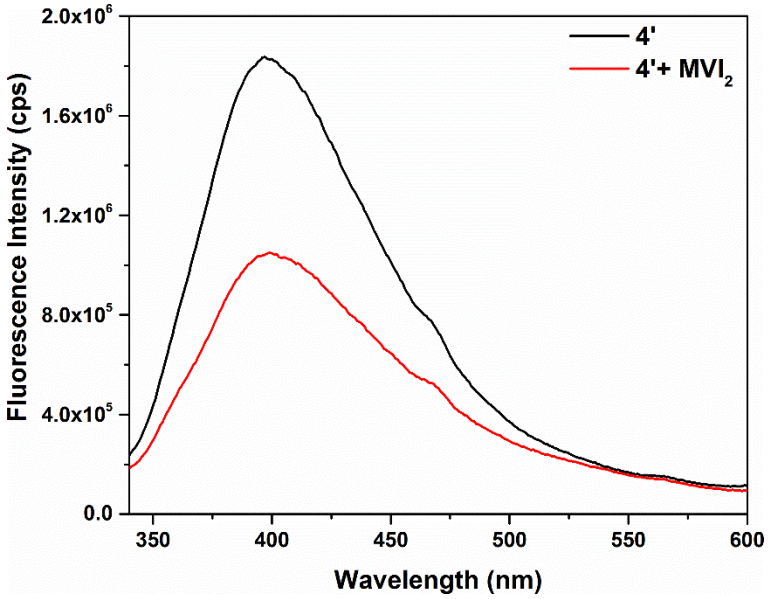

Figure S62. Change in the fluorescence intensity of **4′** in presence of 10 mM MVI_2 (500 µL).

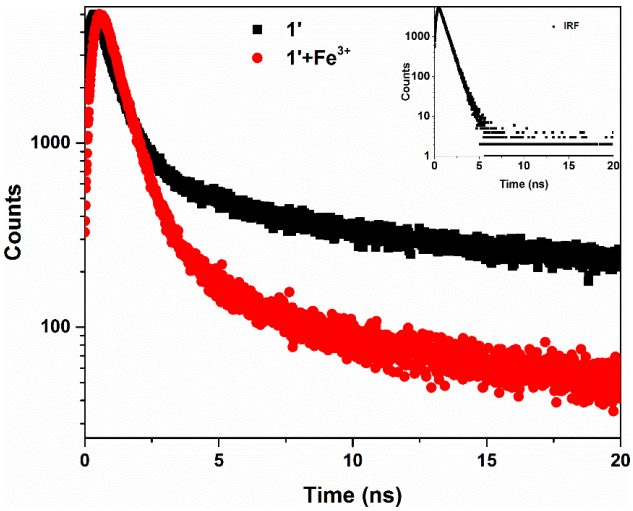

Figure S63. Lifetime decay profile of **1′** in presence of aqueous Fe^{3+} solution (λ_{ex} = 290 nm, monitored at 400 nm).

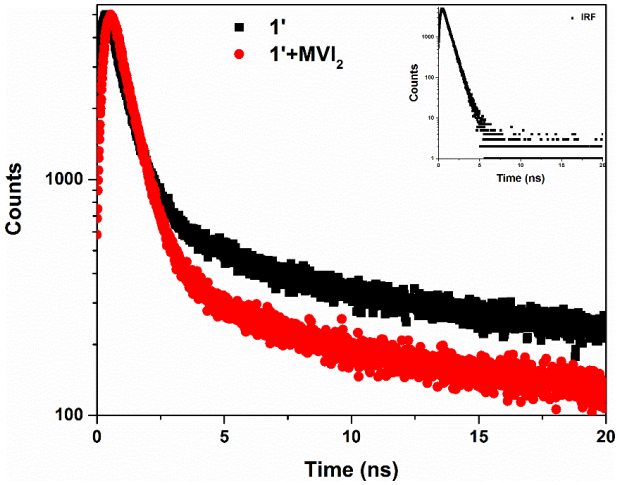

Figure S64. Lifetime decay profile of **1′** in presence of aqueous MVI_2 solution (λ_{ex} = 290 nm, monitored at 400 nm).

Table S4. Excited-state lifetime analysis of **1′** in presence of Fe^{3+} aqueous solution (λ_{ex} = 290 nm, λ_{em} = 400 nm).

Volume of analyte added	τ (ns)			a			Average lifetime (ns) $\langle\tau\rangle$*	χ^2
	τ_1 (ns)	τ_2 (ns)	τ_3 (ns)	a_1	a_2	a_3		
0	16.56	1.72	0.13	0.35	0.09	0.55	6.02	1.03
400 µL (Fe^{3+})	13.06	2.16	0.059	0.21	0.12	0.67	3.03	1.09
400 µL (MVI_2)	10.21	1.79	0.010	0.16	0.11	0.73	1.83	1.05

*$\langle\tau\rangle = a_1\tau_1 + a_2\tau_2 + a_2\tau_2 + a_3\tau_3$

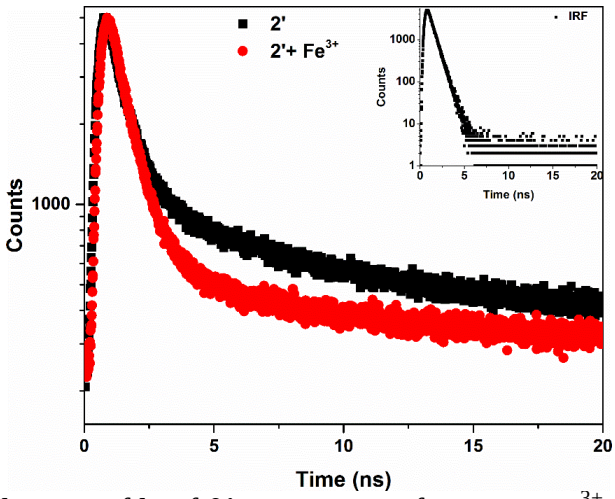

Figure S65. Lifetime decay profile of **2′** in presence of aqueous Fe^{3+} solution (λ_{ex} = 290 nm, monitored at 400 nm).

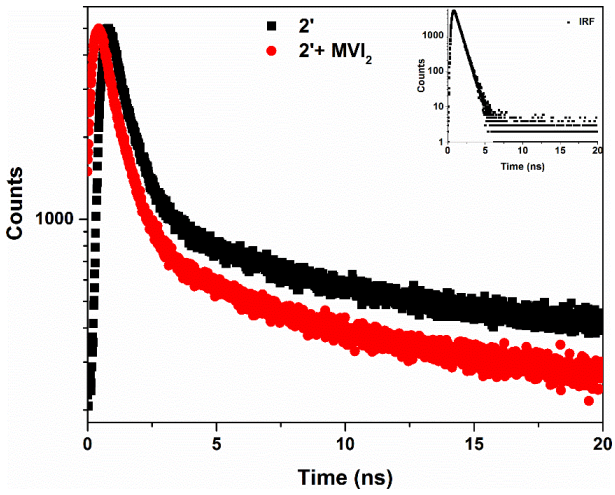

Figure S66. Lifetime decay profile of **2′** in presence of aqueous MVI_2 solution (λ_{ex} = 290 nm, monitored at 400 nm).

Table S5. Excited-state lifetime analysis of **2′** in presence of Fe^{3+} aqueous solution (λ_{ex} = 290 nm, λ_{em} = 400 nm).

Volume of analyte added	τ (ns)			a			Average lifetime (ns) <τ>*	χ^2
	τ_1 (ns)	τ_2 (ns)	τ_3 (ns)	a_1	a_2	a_3		
0	15.44	4.73	0.69	0.50	0.17	0.33	8.77	1.11
400 µL (Fe^{3+})	9.92	0.93	0.06	0.30	0.12	0.58	3.17	1.04
400 µL (MVI_2)	10.31	1.87	0.14	0.16	0.11	0.73	1.94	1.01

*$\langle\tau\rangle = a_1\tau_1 + a_2\tau_2 + a_2\tau_2 + a_3\tau_3$

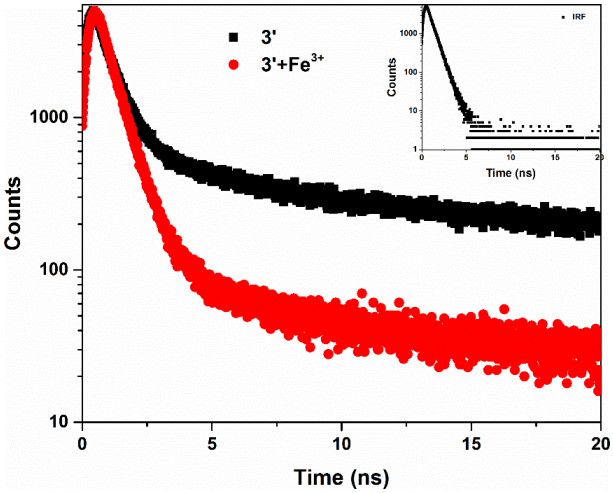

Figure S67. Lifetime decay profile of **3′** in presence of aqueous Fe^{3+} solution (λ_{ex} = 290 nm, monitored at 400 nm).

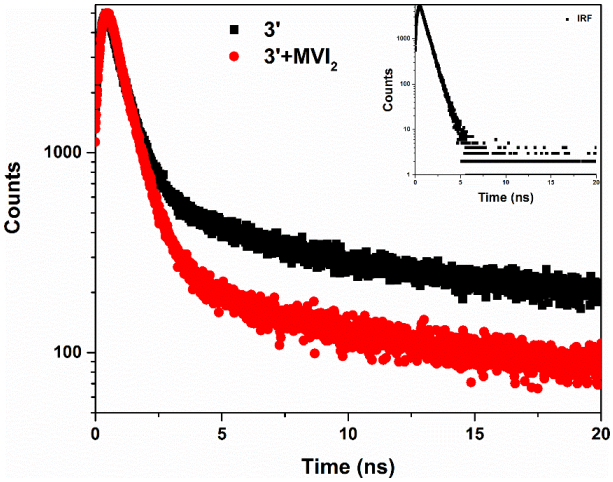

Figure S68. Lifetime decay profile of **3′** in presence of aqueous MVI_2 solution (λ_{ex} = 290 nm, monitored at 400 nm).

Table S6. Excited-state lifetime analysis of **3′** in presence of different analyte in aqueous solution (λ_{ex} = 290 nm, λ_{em} = 400 nm).

Volume of analyte added (400 µL)	τ (ns)			a			Average lifetime (ns) <τ>*	χ^2
	τ_1 (ns)	τ_2 (ns)	τ_3 (ns)	a_1	a_2	a_3		
0	15.95	1.79	0.12	0.37	0.07	0.56	6.10	1.08
400 µL (Fe^{3+})	15.59	1.95	0.105	0.14	0.05	0.81	2.35	1.03
400 µL (MVI_2)	14.95	1.88	0.10	0.28	0.04	0.68	4.32	1.01

*$\langle\tau\rangle = a_1\tau_1 + a_2\tau_2 + a_2\tau_2 + a_3\tau_3$

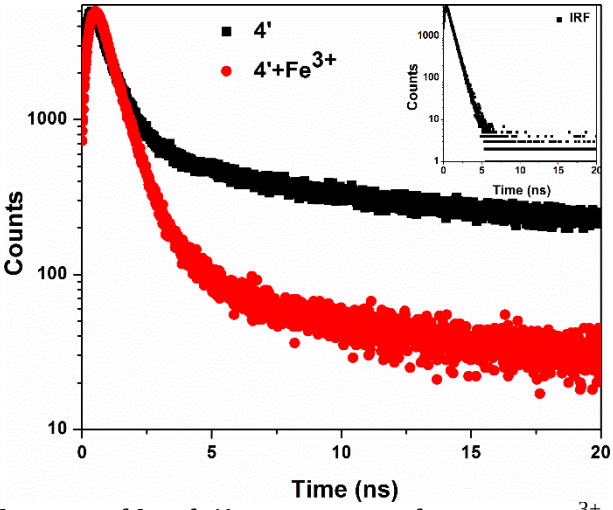

Figure S69. Lifetime decay profile of **4′** in presence of aqueous Fe^{3+} solution (λ_{ex} = 290 nm, monitored at 400 nm).

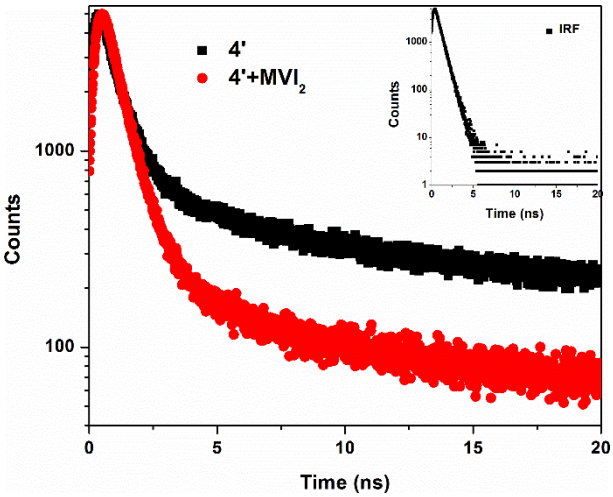

Figure S70. Lifetime decay profile of **4′** in presence of aqueous MVI_2 solution (λ_{ex} = 290 nm, monitored at 400 nm).

Table S7. Excited-state lifetime analysis of **4′** in presence of different analyte in aqueous solution (λ_{ex} = 290 nm, λ_{em} = 400 nm).

Volume of analyte added	τ (ns)			a			Average lifetime (ns) <τ>*	χ^2
	τ_1 (ns)	τ_2 (ns)	τ_3 (ns)	a_1	a_2	a_3		
0	16.71	1.95	0.12	0.33	0.10	0.57	5.8	1.04
400 µL (Fe^{3+})	13.59	1.96	0.10	0.19	0.08	0.73	2.84	1.07
400 µL (MVI_2)	11.37	1.79	0.10	0.25	0.07	0.68	2.99	1.09

*$\langle\tau\rangle = a_1\tau_1 + a_2\tau_2 + a_2\tau_2 + a_3\tau_3$

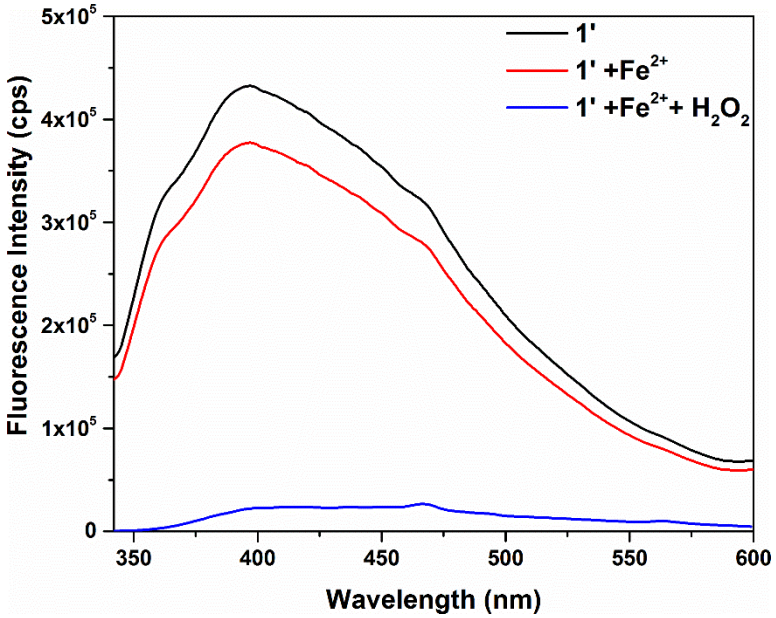

Figure S71. Change in the fluorescence intensity of **1′** upon addition of H_2O_2 solution (1mM) in presence of Fe^{2+} ion (500 µL).

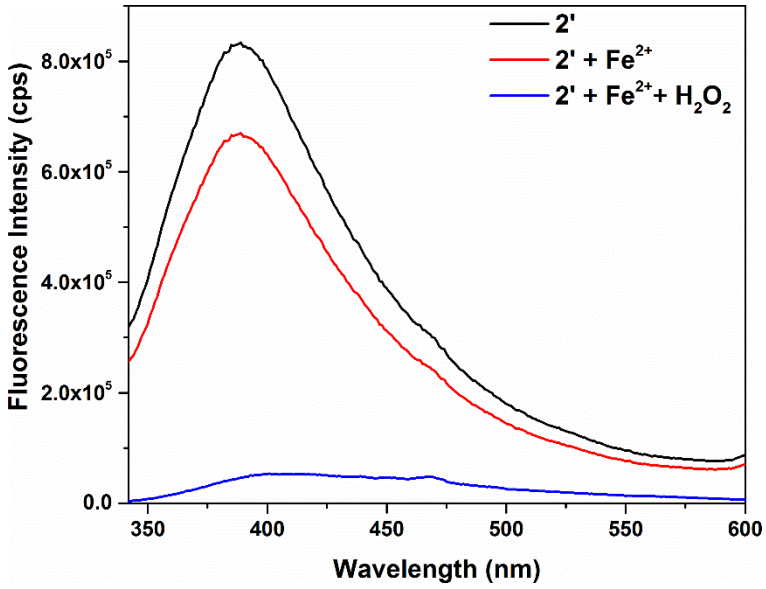

Figure S72. Change in the fluorescence intensity of **2′** upon addition of H_2O_2 solution (1 mM) in presence of Fe^{2+} ion (500 µL).

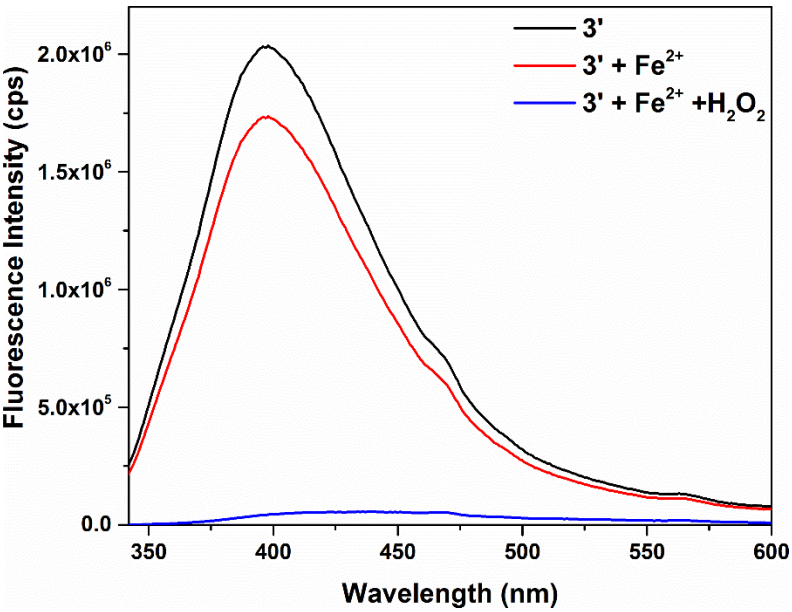

Figure S73. Change in the fluorescence intensity of **3′** upon addition of H_2O_2 solution (1 mM) in presence of Fe^{2+} ion (500 µL).

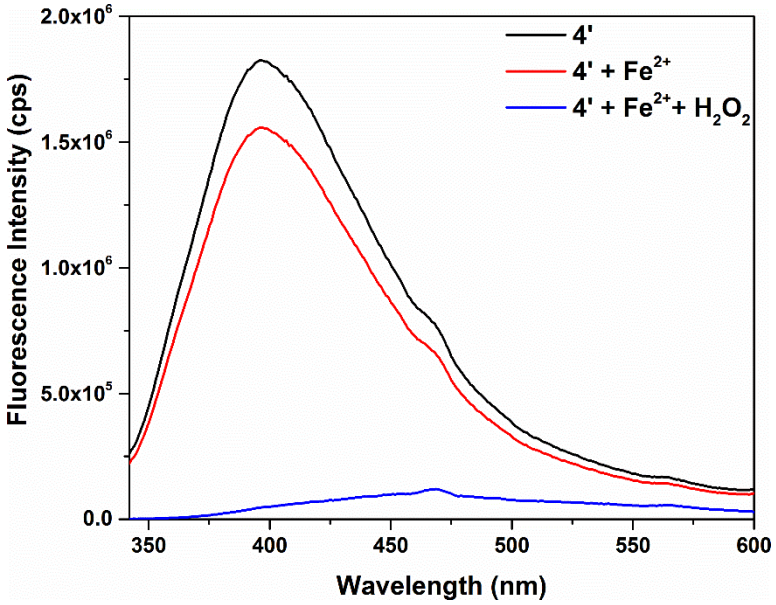

Figure S74. Change in the fluorescence intensity of **4′** upon addition of H_2O_2 solution (1 mM) in presence of Fe^{2+} ion (500 µL).

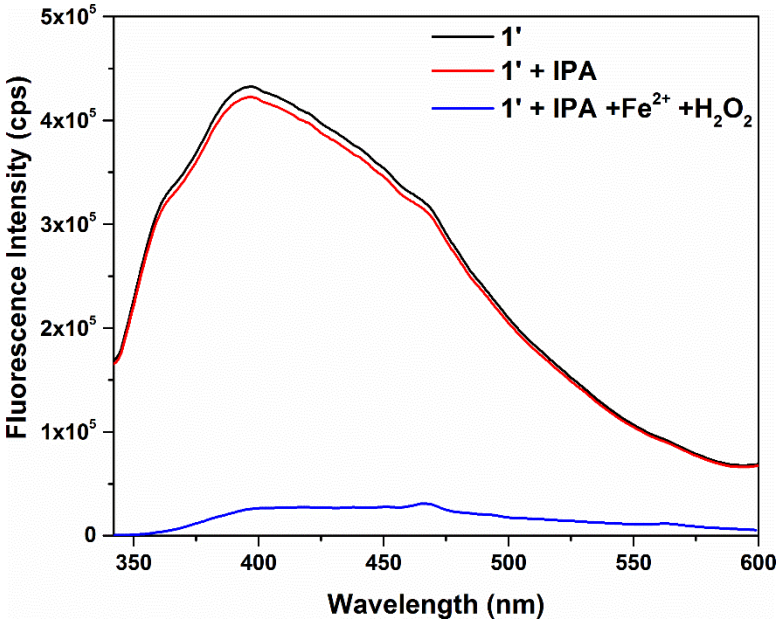

Figure S75. Change in the fluorescence intensity of **1′** upon addition of Fe^{2+}-H_2O_2 solution in presence of IPA (300 µL).

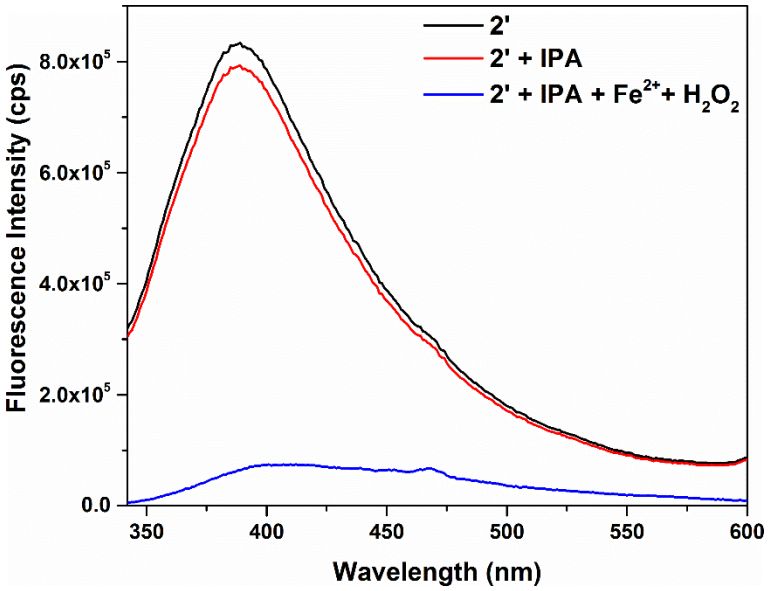

Figure S76. Change in the fluorescence intensity of **2′** upon addition of Fe^{2+}-H_2O_2 solution in presence of IPA (300 µL).

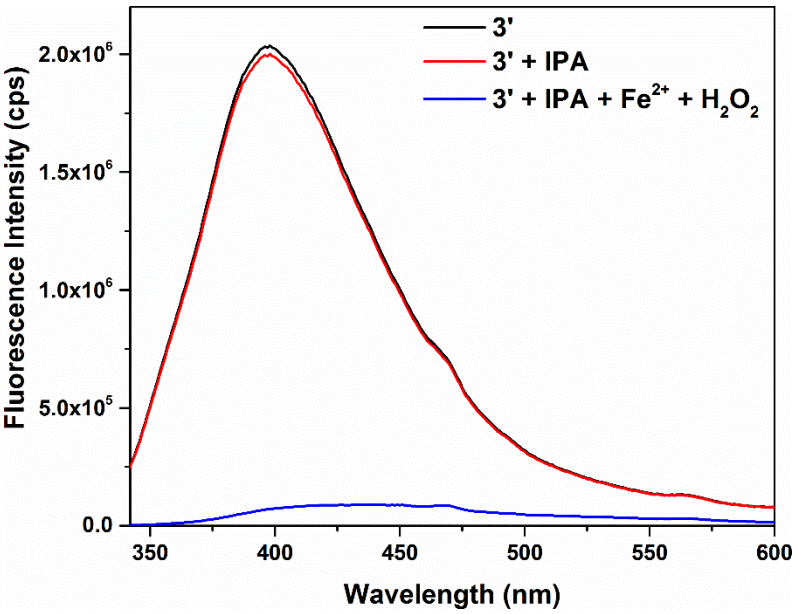

Figure S77. Change in the fluorescence intensity of **3′** upon addition of Fe^{2+}-H_2O_2 solution in presence of IPA (300 µL).

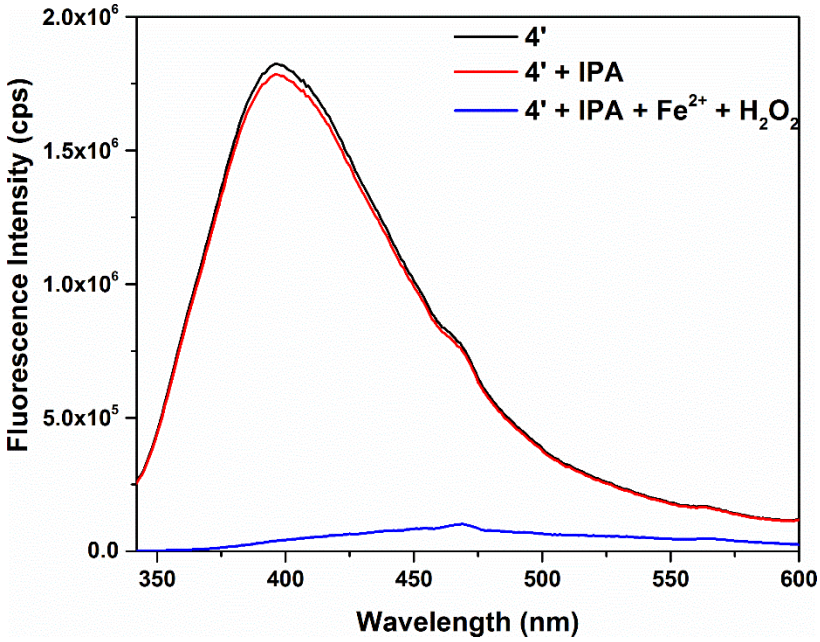

Figure S78. Change in the fluorescence intensity of **4′** upon addition of Fe^{2+}-H_2O_2 solution in presence of IPA (300 µL).

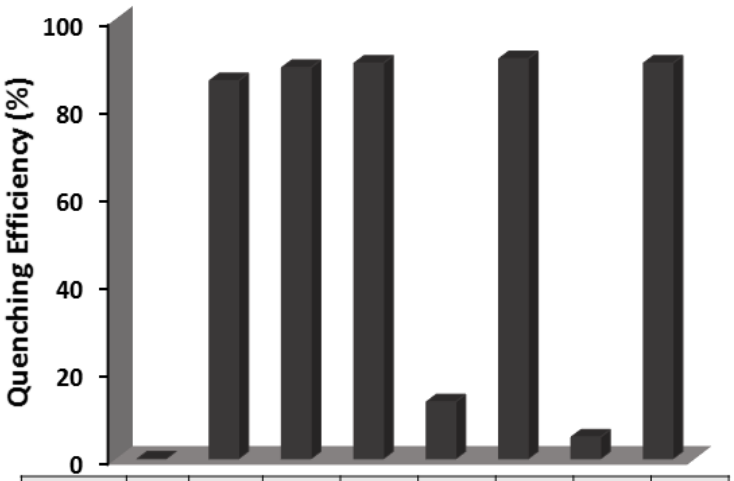

Input 1 (Fe^{3+})	0	1	1	1	0	0	0	1
Input 2 (Fe^{2+})	0	0	1	0	1	1	0	1
Input 3 (H_2O_2)	0	0	0	1	0	1	1	1
Output	0	1	1	1	0	1	0	1

Figure S79. The fluorescence quenching efficiency of **1′** in presence of different input and its corresponding truth table for logic gate construction.

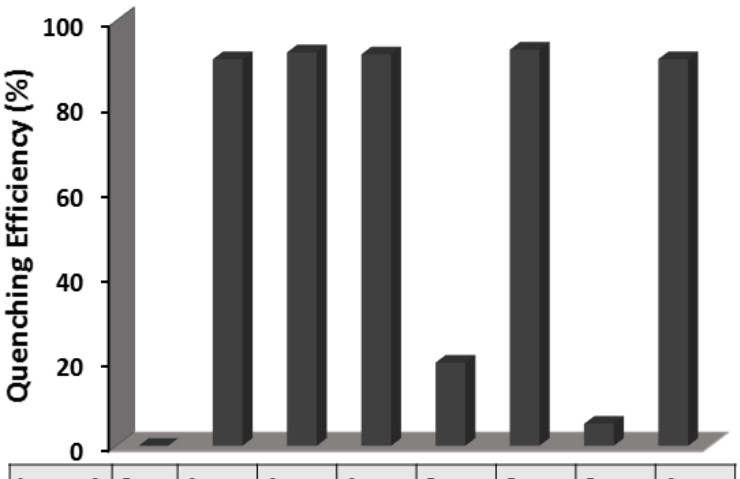

Input 1 (Fe^{3+})	0	1	1	1	0	0	0	1
Input 2 (Fe^{2+})	0	0	1	0	1	1	0	1
Input 3 (H_2O_2)	0	0	0	1	0	1	1	1
Output	0	1	1	1	0	1	0	1

Figure S80. The fluorescence quenching efficiency of **2′** in presence of different input and its corresponding truth table for logic gate construction.

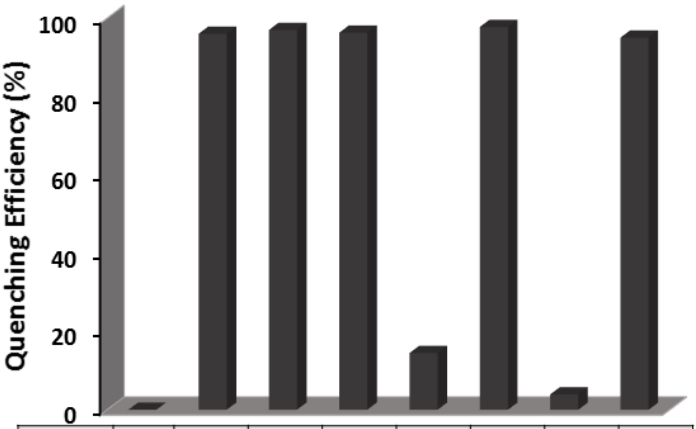

Input 1 (Fe^{3+})	0	1	1	1	0	0	0	1
Input 2 (Fe^{2+})	0	0	1	0	1	1	0	1
Input 3 (H_2O_2)	0	0	0	1	0	1	1	1
Output	0	1	1	1	0	1	0	1

Figure S81. The fluorescence quenching efficiency of **3′** in presence of different input and its corresponding truth table for logic gate construction.

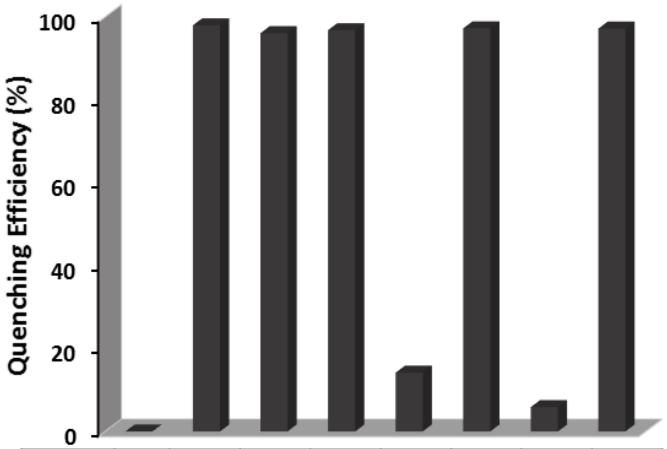

Input 1 (Fe^{3+})	0	1	1	1	0	0	0	1
Input 2 (Fe^{2+})	0	0	1	0	1	1	0	1
Input 3 (H_2O_2)	0	0	0	1	0	1	1	1
Output	0	1	1	1	0	1	0	1

Figure S82. The fluorescence quenching efficiency of **4′** in presence of different input and its corresponding truth table for logic gate construction.

References:

[1] S. Mostakim, M. Grzywa, D. Volkmer and S. Biswas, *J. Solid State Chem.* **2015**, 232, 221-227.
[2] K. Wang, H. Huang, W. Xue, D. Liu, X. Zhao, Y. Xiao, Z. Li, Q. Yang, L. Wang and C. Zhong, *CrystEngComm* **2015**, 17, 3586-3590.
[3] C. Zhang, Y. Yan, Q. Pan, L. Sun, H. He, Y. Liu, Z. Liang and J. Li, *Dalton Trans.* **2015**, 44, 13340-13346.
[4] Y.-F. Li, D. Wang, Z. Liao, Y. Kang, W.-H. Ding, X.-J. Zheng and L.-P. Jin, *J. Mater. Chem. C* **2016**, 4, 4211-4217.
[5] M. Zheng, H. Tan, Z. Xie, L. Zhang, X. Jing and Z. Sun, *ACS Appl. Mater. Interfaces* **2013**, 5, 1078-1083.
[6] X.-H. Zhou, L. Li, H.-H. Li, A. Li, T. Yang and W. Huang, *Dalton Trans.* **2013**, 42, 12403-12409.
[7] Y. Wu, G.-P. Yang, Y. Zhang, N. Shi, J. Han and Y.-Y. Wang, *RSC Adv.* **2015**, 5, 90772-90777.
[8] X.-L. Zhao, D. Tian, Q. Gao, H.-W. Sun, J. Xu and X.-H. Bu, *Dalton Trans.* **2016**, 45, 1040-1046.
[9] K.-M. Wang, L. Du, Y.-L. Ma, J.-S. Zhao, Q. Wang, T. Yan and Q.-H. Zhao, *CrystEngComm* **2016**, 18, 2690-2700.
[10] X.-Y. Xu and B. Yan, *ACS Appl. Mater. Interfaces* **2014**, 7, 721-729.
[11] C.-X. Yang, H.-B. Ren and X.-P. Yan, *Anal. Chem.* **2013**, 85, 7441-7446.
[12] G.-P. Li, G. Liu, Y.-Z. Li, L. Hou, Y.-Y. Wang and Z. Zhu, *Inorg. Chem.* **2016**, 55, 3952-3959.
[13] H. Xu, H.-C. Hu, C.-S. Cao and B. Zhao, *Inorg. Chem.* **2015**, 54, 4585-4587.
[14] X.-Y. Dong, R. Wang, J.-Z. Wang, S.-Q. Zang and T. C. Mak, *J. Mater. Chem. A* **2015**, 3, 641-647.
[15] H. Weng and B. Yan, *Sens. Actuator B-Chem.* **2016**, 228, 702-708.